Journal of Quantitative Spectroscopy & Radiative Transfer 309 (2023) 108708

Contents lists available at ScienceDirect

Journal of Quantitative Spectroscopy & Radiative Transfer

journal homepage: www.elsevier.com/locate/jqsrt

Prediction of the radiation characteristics and the light absorption rate of *Chlamydomonas reinhardtii* cultivated under a progressive nitrogen starvation and accumulating carbon reserves

Fernando Robert Ferrel Ballestas[a,b], Mariana Titica[a], Jack Legrand[a], Laurent Pilon[c,d,e], Guillaume Cogne[a,*]

[a] Nantes Université, Oniris, CNRS, GEPEA, UMR 6144, F-44600 Saint-Nazaire, France
[b] Laboratorio de Biotecnología, Sede de investigación universitaria, Universidad de Antioquia, Medellín, Colombia
[c] Mechanical and Aerospace Engineering Department, University of California, Los Angeles, Los Angeles, CA 90095-1597, USA
[d] California NanoSystems Institute, University of California, Los Angeles, Los Angeles, CA 90095, USA
[e] Institute of the Environment and Sustainability, University of California, Los Angeles, Los Angeles, CA 90095, USA

ARTICLE INFO

Article history:
Received 23 January 2023
Revised 5 June 2023
Accepted 20 June 2023
Available online 21 June 2023

Keywords:
Radiation characteristics
Starch
Light absorption
Nitrogen starvation
Microalgae
Photobioreactors

ABSTRACT

This paper aims to develop a new method to predict the radiation characteristics of the green microalgae *C. reinhardtii* during progressive nitrogen starvation that accounts for the physiological changes induced by nutritional stress. First, the radiation characteristics of *C. reinhardtii* cultivated under progressive nitrogen starvation were predicted in the photosynthetically active radiation (PAR) region based on Lorenz–Mie theory using effective spectral optical properties of cells accounting for pigment contents, cessation of cell division, cell volume and size, and carbon reserve storage in the form of starch. The predictions of the spectral mass absorption and scattering cross-sections agreed very well with experimental measurements for a wide range of starch mass fractions. Second, the predicted and measured radiation characteristics were used to determine the local rate of photon absorption (LRPA) in the PAR region using the two-flux approximation and simplified two-flux approximation. The LRPA PAR-averaged relative difference between experimental calculation and numerical predictions was less than 9% for all starch mass content considered. In addition, the influence of the mass scattering cross-section on the PAR-averaged LRPA was found to be negligible despite the starch accumulation in microalgae cells. Finally, the numerically-validated tools developed in this study could be used for generating a database of radiation characteristics helpful in order to model growth and carbon reserve accumulation kinetics in microalgae.

1. Introduction

Microalgae have the ability to sequester CO_2 and convert solar energy absorbed in the photosynthetically active radiation (PAR) region into chemical energy *via* photosynthesis. Several strains are metabolically "equipped" to synthesize value-added molecules including pigments, polysaccharides such as starch, lipids to be converted into biodiesel, and biohydrogen [1–3]. In fact, although the biomass of microalgae has been studied and used in different fields (e.g., food, cosmetics, pharmaceuticals) [1,4], their contemporary significance is, arguably, as a sustainable source of biofuels.

Particular focus has been placed on microalgal biomass as feedstock for next generation biofuels. Nutrient limitation or deprivation is the typical method used to induce the accumulation of carbon reserves in the form of starch and/or lipids within the cells. Indeed, the metabolic response of microalgae to deficient culture conditions in terms of elements such as N, S, P, Ca, and Mg, can be quite complex [5]. A deficiency in one of these elements induces a decrease in photosynthetic activity due to the degradation of the photosystems, the cessation of the cell division, and the storage of carbon reserves (e.g., sugars and lipids) [5]. Moreover, if the nutritional stress is carried out under anoxic conditions, then biohydrogen production can be observed [5].

Nitrogen is often considered to carry out nutritional limitation or starvation in microalgae cultures [6,7]. In fact, during a nitrogen-stressed culture, generally a starch-accumulation phase occurred first to give way to triacylglycerides (TAG) accumulation once starch levels reached a certain threshold [8–10]. Thus, controlling the starch-accumulation phase has appeared to be cru-

* Corresponding author.
E-mail address: guillaume.cogne@univ-nantes.fr (G. Cogne).

https://doi.org/10.1016/j.jqsrt.2023.108708
0022-4073/

Nomenclature

$\mathcal{A}$	local rate of photon absorption, mol_{hv}/kgh
$\langle \mathcal{A} \rangle$	mean specific rate of photon absorption, mol_{hv}/kgh
$\bar{A}_{abs,\lambda}$	average mass spectral absorption cross section, m^2/kg
b_λ	backward scattering ratio
$\bar{C}_{abs,\lambda}$	average cell spectral absorption cross section, m^2
$\bar{C}_{sca,\lambda}$	average cell spectral scattering cross section, m^2
C	concentration, kg/m^3
Ea	specific absorption cross-section of individual pigments, m^2/kg
f	frequency
f_v	volume fraction
G_λ	fluence rate using total biomass, $\mu mol_{hv}/m^2s$
G'_λ	fluence rate using catalytic biomass, $\mu mol_{hv}/m^2s$
l	optical thickness
m_{XC}	mass of one individual cell, kg
m_λ	spectral complex refractive index
n_{v_p}	refractive index at the anchor point
n_λ	spectral refractive index
N_T	cell density, #/mL
$q_{\lambda,0}$	incident spectral radiation, $\mu mol/m^2s$
r_{eq}	cell equivalent radius, µm
$\bar{r}_{eq}$	mean cell equivalent radius, µm
$\bar{S}_{sca,\lambda}$	average mass spectral scattering cross section, m^2/kg
T	transmittance
V	volume, m^3
w	mass fraction
w_{pig}	pigment mass fraction based on total biomass concentration, wt.%
w'_{pig}	pigment mass fraction based on catalytic biomass concentration, wt.%
w''_{pig}	pigment mass fraction within total pigment concentration, wt.%
x_w	water fraction in cells
z	photobioreactor depth, m

Greek symbols

β_λ	spectral extinction coefficient, m^{-1}
ε_n	scattering correction factor
ε_h	contribution of the forward scattered light to $T_{nh,\lambda,C_{XT}}$
Θ	scattering angle, rad
Θ_a	acceptance angle of the detector, rad
ρ_{dry}	dry biomass density, kg/m^3
ρ_λ	diffuse reflectance of the PBR back wall
κ_λ	spectral absorption coefficient, m^{-1}
λ	refers to wavelength, nm
$\sigma_{s,\lambda}$	spectral scattering coefficient, m^{-1}
σ	standar deviation, µm
$\Phi_{T,\lambda}$	scattering phase function

Subscripts

abs	refers to absorption
basal	refers to basal or starting value
cell	refers to cell particle
Chl	refers to total chlorophylls
Chla	refers to chlorophyll *a*
Chlb	refers to chlorophyll *b*
CR	refers to cultivating conditions leading to carbon reserves accumulation
eff	refers to effective properties
hv	refers to photons of light
LRPA	refers to local rate of photon absorption
MeOH	refers to methanol
nn	refers to normal-normal configuration
nh	refers to normal-hemispherical configuration
PAR	refers to averaged over the PAR region
PBR	refers to photobioreactor
PBS	refers to phosphate buffer saline solution
pig	refers to pigments
PhPC	refers to photoprotective carotenoids
PSC	refers to photosynthetic carotenoids
PPC	refers to photoprotective and photosynthetic carotenoids
r	refers to carbon reserves
ref	refers to reference
sca	refers to scattering
simp	refers to simplified
s	refers to sample
st	refers to starch
TAG	refers to triacylglycerides
T	refers to total
V	refers to volume
XT	refers to total biomass
XC	refers to catalytic biomass

cial for the production of both biodiesel and biohydrogen. Many metabolic studies have demonstrated that starch accumulation is used by microalgae as precursor for lipid production during nitrogen-limiting conditions [9–11]. Similarly, the degradation of starch accumulated during sulfur-deprived culture was shown to play an important role in biohydrogen production [12,13].

Nitrogen-limited cultures are typically grown in photobioreactors (PBRs) with artificial light or sunlight. Several kinetic models have been proposed and validated for coupling light transfer in PBR to biomass, starch, and lipids productivities [8,14–17]. These models are important to perform technoeconomic analysis and sustainability assessment, to optimize microalgal bioprocesses, as well as to scale-up the process from benchtop to industrial scales. These models require knowledge of the microalgae radiation characteristics over the PAR region to predict the local fluence rate and the local rate of photon absorption (LRPA).

Experimental methods have been developed for measuring the radiation characteristics of microalgae suspensions for cells of any arbitrary shape [18,19]. Note that the radiation characteristics measurements must be repeated for each medium composition and growth conditions including pH, temperature, and illumination. This is particularly true when nutritional stress is imposed such as nitrogen starvation resulting in time-dependent cell composition and pigment content [20–23].

Radiation characteristics of quasi-spherical microalgae can be also be predicted theoretically based on the Lorenz–Mie theory [24–28]. The cells are approximated as homogeneous spheres with volume-equivalent radius and effective spectral complex index of refraction $m_\lambda = n_\lambda + ik_\lambda$ where n_λ and k_λ are the cell's effective refractive and absorption indices, respectively. For spherical cells with a strongly refracting wall, the cells can be treated as coated spheres while filamentous cells can be treated as infinity long and randomly oriented cylinders [29–31]. Difficulties in predicting the radiation characteristics of microalgae lie in the fact that the cell size and biochemical compositions (e.g., pigment, starch, or lipid concentrations) may change during nutritional limitations.

This study aims to develop a theoretical model capable of predicting the spectral radiation characteristics over the PAR-region of green microalgae *C. reinhardtii* cultivated under progressive nitro-

gen starvation and accumulation of carbon reserves in the form of starch. Predictions were compared with experimental measurements over the PAR region as microalgae underwent physiological changes in the pigment and starch concentrations, cell volume and size, and cessation of cell division. The results were then used to predict changes in the LRPA under these various conditions.

2. Current state of knowledge

2.1. Chlamydomonas reinhardtii

C. reinhardtii is an eukaryotic unicellular green microalgae with an oblate spheroid shape measuring about 8–10 μm in diameter [32]. It is considered as a model organism used as a biological platform to study physiological and metabolic processes such as biogenesis, photosynthesis, stress responses, and regulatory mechanisms [5,32]. Like in many other green microalgae, the photosynthetic pigments of *C. reinhardtii* are composed of chlorophyll *a* (Chl *a*) and b (Chl *b*) along with photoprotective and photosynthetic carotenoids (PPC). Pigment light absorption take place in the PAR region and the spectral absorption peaks of Chl *a* and *b* are centered at 435, 630, and 676 nm and those of PPC present between 400 and 500 nm [19].

The interest in *C. reinhardtii* is primarily due to its potential to produce renewable biofuels. Indeed, thanks to its ability to grow under various conditions (autotrophic, heterotrophic, and mixotrophic conditions), *C. reinhardtii* can accumulate large amounts of carbon storage molecules such as starch and/or triacylegliceride (TAGs) under nutritionally deficient conditions. It can also acclimate to prolong anaerobiosis conditions both under light and dark conditions to produce biohydrogen [5].

The impact of light on the biomass growth as well as on the production of metabolites of interest, such as lipids or pigments, have been studied extensively for the green microalgae *C. reinhardtii* for two purposes (1) to optimize the operation protocols and (2) for kinetics modeling [16,17,21,22,33,34]. Determination of the radiation characteristics of *C. reinhardtii* has been carried out under optimal growth [18,25,26,35] and nitrogen-limitation conditions [35]. However, previous studies conducted under nitrogen-stress conditions did not consider the effect of accumulation of carbon reserves on the radiation characteristics of *C. reinhardtii*.

2.2. Determination of the radiation characteristics of microalgae culture

2.2.1. Experimental measurements

Pilon et al. [18] presented a method to measure experimentally the radiation characteristics of microalgae suspensions based on three assumptions: (*i*) the microalgae suspension was well mixed and the cells were randomly oriented, (*ii*) the suspension was sufficiently diluted to ensure that single scattering prevailed, and (*iii*) the scattering phase function was assumed to be essentially in the forward direction, time-invariant, and independent of wavelength over the PAR region.

The average mass absorption and scattering cross-section $\bar{A}_{abs,\lambda}$ and $\bar{S}_{sca,\lambda}$ of a microalgae suspension can be defined as in terms of total dry biomass concentration C_{XT} [18]

$$\bar{A}_{abs,\lambda} = \frac{\kappa_\lambda}{C_{XT}} \text{ and } \bar{S}_{sca,\lambda} = \frac{\sigma_{s,\lambda}}{C_{XT}} \left(\text{inm}^2/\text{kgdry weight}\right) \quad (1)$$

where, κ_λ and $\sigma_{s,\lambda}$ are the absorption and scattering coefficients (in m^{-1}), respectively. The apparent extinction β^*_λ and absorption κ^*_λ coefficients can be obtained from normal-normal $T_{nn,\lambda,C_{XT}}$ and normal-hemispherical $T_{nh,\lambda,C_{XT}}$ transmittance measurements for different diluted microalgae suspensions of known total biomass concentration C_{XT} placed in a cuvette of pathlength l according to [18]

$$\beta^*_\lambda = -\frac{1}{l}\ln\left(\frac{T_{nn,\lambda,C_{XT}}}{T_{nn,\lambda,ref}}\right) \text{ and } \kappa^*_\lambda = -\frac{1}{l}\ln\left(\frac{T_{nh,\lambda,C_{XT}}}{T_{nh,\lambda,ref}}\right) \quad (2)$$

where, $T_{nn,\lambda,\,ref}$ and $T_{nh,\lambda,\,ref}$ are the normal-normal and normal-hemispherical transmittances of the medium alone in the cuvette, respectively. Microalgae are usually suspended in phosphate buffer saline (PBS) solution to eliminate any absorption and scattering by the medium [18].

The apparent extinction coefficient β^*_λ can be expressed in terms of the actual absorption κ_λ and scattering $\sigma_{s,\lambda}$ coefficients as [18]

$$\beta^*_\lambda = \kappa_\lambda + (1-\epsilon_n)\ \sigma_{s,\lambda}. \quad (3)$$

Here, ε_n is a correction factor representing the fraction of light scattered in the forward direction and detected by the spectrometer. Under ideal conditions, ε_n is equal to zero so that $\beta^*_\lambda = \beta_\lambda$. However, the acceptance angle Θ_a of the detector is finite so ε_n is strictly positive and is assumed to be constant over the PAR region. It can be calculated from the suspension's scattering phase function $\Phi_{T,\lambda}(\Theta)$ as [18]

$$\epsilon_n = \frac{1}{2}\int_0^{\frac{\Theta_a}{2}} \Phi_{T,\lambda}(\Theta) sin\Theta d\Theta. \quad (4)$$

The correction factor ε_n for *C. reinhardtii* suspensions cultivated under optimal and nitrogen-limiting conditions was reported as 0.67 and 0.72, respectively [35]. Thus, the correction factor ε_n does not seem to be affected significantly by nitrogen limitation. Then, the actual extinction coefficient $\beta_\lambda = \kappa_\lambda + \sigma_{s,\lambda}$ can be determined according to [18]

$$\beta_\lambda = \frac{\beta^*_\lambda - \epsilon_n\kappa_\lambda}{1-\epsilon_n}. \quad (5)$$

Similarly, the apparent absorption coefficient κ^*_λ is related to the actual absorption coefficient κ_λ and scattering $\sigma_{s,\lambda}$ coefficient according to [18]

$$\kappa^*_\lambda = \kappa_\lambda + (1-\epsilon_h)\ \sigma_{s,\lambda}. \quad (6)$$

Here, ε_h corresponds to the scattered light fraction measured by the detector connected to the integrating sphere. In particular, when all the scattered light is accounted for, ε_h is equal to 1. Moreover, at $\lambda = 750$ nm green microalgae are known to be non-absorbing, *i.e.*, $\kappa_{750} = 0\ m^{-1}$. Then, evaluating Eqs. (5) and (6) at this wavelength yield ε_h and the actual absorption κ_λ and scattering coefficients $\sigma_{s,\lambda}$ can be expressed as [18]

$$\kappa_\lambda = \kappa^*_\lambda - \kappa^*_{750}\left(\frac{\beta^*_\lambda - \kappa^*_\lambda}{\beta^*_{750} - \kappa^*_{750}}\right) \text{ and } \sigma_{s,\lambda} = \beta_\lambda - \kappa_\lambda. \quad (7)$$

The mass cross-sections $\bar{A}_{abs,\lambda}$ and $\bar{S}_{sca,\lambda}$ determined by this method are independent of the biomass concentration. Indeed, single scattering must prevail, *i.e.*, photons undergo at most one scattering event as they travel through the microalgae suspension. In practice, it is verified that single scattering prevails by repeating the measurements for two or three diluted microalgae suspensions with different biomass concentrations [19].

2.2.2. Theoretical predictions

C. reinhardtii cells growing under non-limiting conditions have been successfully modeled as homogeneous spheres with effective complex index of refraction $m_\lambda = n_\lambda + ik_\lambda$ and size distribution $f(r_{eq})$ where r_{eq} is the volume-equivalent radius [24–28,35]. In fact, it has been demonstrated that *C. reinhardtii* can be treated as homogeneous spherical particles despite their heterogeneous cell composition [36]. It is important to mention that unlike other green microalgae such as *Chlorella sp.*, *Chlamydomonas reinhardtii* does not have a cell wall but only a cell membrane whose optical

effects are negligible [35]. Then, theoretical predictions of their average absorption $\bar{C}_{abs,\lambda}$ and scattering $\bar{C}_{sca,\lambda}$ cross-sections (in m^2) as well as the scattering phase function $\Phi(r_{eq},\Theta)$ can be obtained by the Lorenz–Mie theory. In order to couple metabolic response of microalgae and light transfer so as to predict biomass productivity and concentration evolution in photobioreactors, one can consider the average mass absorption $\bar{A}_{abs,\lambda}$ and scattering $\bar{S}_{sca,\lambda}$ cross-section defined as [25]

$$\bar{A}_{abs,\lambda} = \frac{\bar{C}_{abs,\lambda}}{V_{32}\rho_{dry}(1-x_w)} \text{ and}$$

$$\bar{S}_{sca,\lambda} = \frac{\bar{C}_{sca,\lambda}}{V_{32}\rho_{dry}(1-x_w)} \left(\text{in } m^2/\text{kg dry weight}\right) \quad (8)$$

where, V_{32} (in m^3) is the Sauter mean volume of the cell, ρ_{dry} = 1400 kg/m^3 is the density of dry biomass, and x_w = 0.8 is the average mass fraction of water in the cells [25].

The methodology used for the theoretical predictions of radiation characteristics of microalgae cells has been described in detail in Refs. [26,35]. First, the cells effective absorption index k_λ can be calculated according to [25]

$$k_\lambda = \frac{\lambda}{4\pi}\sum_j C_{pig,j}Ea_j = \frac{\lambda}{4\pi}\rho_{dry}(1-x_w)\sum_j w_{pig,j}Ea_j \quad (9)$$

where, $C_{pig,j}$ is the concentration of jth pigment in the cell (in kg/m^3), while $w_{pig,j} = C_{pig,j}/C_{XT}$ is the mass fraction of the jth pigment in the total biomass. Moreover, Ea_j (in m^2/kg) is the specific absorption cross-section of any pigment j reported by Bidigare et al. [37]. Note that this expression has been validated experimentally for *C. reinhardtii* cultures cultivated under non-limiting nutritional conditions [19,25,26,35].

Second, the spectral refractive index n_λ of *C. reinhardtii* can be assumed to be constant over the PAR region and equal to 1.55 [25]. Dauchet et al. [26] relaxed this assumption and predicted the spectral refractive index n_λ using the subtractive Kramers–Kronig relation, based on the spectral absorption index $k_\lambda = k_\nu$ given by Eq. (9) according to [26]

$$n_\lambda = n_{\nu_p} + 2\frac{\nu^2-\nu_p^2}{\pi}P\int_{\nu_{min}}^{\nu_{max}}\frac{\nu' k_{\nu'}}{(\nu'-\nu^2)(\nu'-\nu_p^2)}d\nu' \quad (10)$$

where, $\nu = c/\lambda$ is the frequency of the electromagnetic wave, c is the speed of light in vacuum, and P is the Cauchy principal value. Here, ν_p is the so-called anchor frequency selected such that the cell absorption index vanished, *i.e.*, $k_{\nu_p} = 0$. Moreover, the anchor refractive index n_{ν_p} must be known or retrieved experimentally. Dauchet et al. [26] retrieved a value of n_{ν_p} = 1.44 for the green microalgae *C. reinhardtii* using an inverse method consisting in minimizing the difference between the experimentally measured and the theoretically predicted normal-hemispherical transmittance at 820 nm. Predictions were obtained by solving the RTE using the Monte Carlo method and the predicted radiation characteristics of the spherical microalgae predicted by Lorenz–Mie theory.

On the other hand, Lee et al. [38] retrieved the complex index of refraction of *C. reinhardtii* cultivated under non-limiting nutritional conditions using an inverse method minimizing the difference between predictions by the Lorenz–Mie theory using the measured surface area equivalent cell radius distribution $f(r_{eq})$ and the experimentally measured spectral mass cross-sections $\bar{A}_{abs,\lambda}$ and $\bar{S}_{sca,\lambda}$. The retrieved refractive index n_λ was in the range of 1.35–1.37 over the PAR region.

Finally, Kandilian et al. [35] compared the theoretically determined and experimentally measured radiation characteristics of *C. reinhardtii* cultivated under limiting and non-limiting nitrogen conditions using the Kramers–Kronig relation with two different anchor refractive index, n_{ν_p} = 1.37 and n_{ν_p} = 1.44 at the anchor frequency ν_p of 820 nm. The comparison showed that the prediction of the average mass spectral absorption cross-section $\bar{A}_{abs,\lambda}$ for *C. reinhardtii* growing whether under nitrogen-limiting conditions or optimal conditions were quite similar for the two values of n_{ν_p} considered. Thus, the nutritional growing conditions and the choice of the anchor refractive index n_{ν_p} did not have a significant influence on the theoretical predictions of $\bar{A}_{abs,\lambda}$. Predictions of the mass absorption cross-section $\bar{A}_{abs,\lambda}$ for *C. reinhardtii* grown under nitrogen-limiting conditions agreed relatively well with the measurements with a PAR-averaged relative difference of 14–16%. However, the relative difference between predictions and measurements of $\bar{A}_{abs,\lambda}$ reached up to 53% between 450 and 550 nm corresponding to the absorption band of photosynthetic and photoprotective carotenoid pigments. On the other hand, the mass scattering cross-section $\bar{S}_{sca,\lambda}$ was slightly better predicted with n_{ν_p} equal to 1.44 compared to n_{ν_p} equal to 1.37. Note that Kandilian et al. [35] reported the radiation characteristics of *C. reinhardtii* cultivated under optimal and nitrogen-limiting conditions at arbitrary times. However, the authors did not specify the stress degree due to nitrogen deprivation in the culture and ignored the impact of carbon reserve content on the predictions of $\bar{A}_{abs,\lambda}$ and $\bar{S}_{sca,\lambda}$.

2.3. Light transfer modeling in photobioreactors

Microalgae culture suspension is considered as an absorbing and scattering media in which the spectral light attenuation profile is given by the local fluence rate $G_\lambda(z)$. It can be obtained by solving the radiative equation (RTE) using various methods depending on the PBR geometry. For a one-dimensional flat-plate PBR filled with microalgae suspension scattering strongly in the forward direction, it has been demonstrated that the two-flux approximation provides satisfactory predictions of the local fluence rate $G_\lambda(z)$ given in mol_{hv}/m^2h at depth z expressed as [17,25,34]

$$\frac{G_\lambda(z)}{q_{\lambda,0}} = 2\frac{\left[\rho_\lambda(1+\alpha_\lambda)e^{-\delta_\lambda L} - (1-\alpha_\lambda)e^{-\delta_\lambda L}\right]e^{\delta_\lambda z} + \left[(1+\alpha_\lambda)e^{\delta_\lambda L} - \rho_\lambda(1-\alpha_\lambda)e^{\delta_\lambda L}\right]e^{-\delta_\lambda z}}{(1+\alpha_\lambda)^2e^{\delta_\lambda L} - (1-\alpha_\lambda)^2e^{-\delta_\lambda L} - \rho_\lambda\left(1-\alpha_\lambda^2\right)e^{\delta_\lambda L} + \rho_\lambda\left(1-\alpha_\lambda^2\right)e^{-\delta_\lambda L}}. \quad (11)$$

where, $q_{\lambda,0}$ is the incident spectral radiation flux and ρ_λ is the diffuse reflectance of the PBRs back wall and the coefficients α_λ and δ_λ are defined as [25]

$$\alpha_\lambda = \sqrt{\frac{\bar{A}_{abs,\lambda}}{\bar{A}_{abs,\lambda} + 2b_\lambda\bar{S}_{sca,\lambda}}} \text{ and}$$

$$\delta_\lambda = C_{XT}\sqrt{\bar{A}_{abs,\lambda}\left(\bar{A}_{abs,\lambda} + 2b_\lambda\bar{S}_{sca,\lambda}\right)}. \quad (12)$$

Here, $\bar{A}_{abs,\lambda}$ and $\bar{S}_{sca,\lambda}$ are the average mass absorption and scattering cross-sections (in m^2/kg_{XT}) of the microalgae in suspension, respectively. The backward scattering ratio b_λ is approximately constant over the PAR region and is estimated from the microalgae scattering phase function $\Phi_{T,\lambda}(\Theta)$.

The experimental measurements and theoretical predictions of b_λ for a culture of *C. reinhardtii* cultivated under nitrogen-limiting conditions were reported by Kandilian et al. [35]. The authors measured b_λ = 0.008 for *C. reinhardtii* grown in either optimal or nitrogen-limited conditions compared with theoretical predictions of b_λ = 0.007. These results indicate that b_λ was nearly zero due to strongly forward scattering of the light by the large *C. reinhardtii* cells and that the nitrogen limitation did not affect b_λ. Then, the expression of the fluence rate given by Eqs. (11) and (12) can be simplified by considering that $b_\lambda \approx 0$ as α_λ tends to unity, and

$\delta_\lambda = \bar{A}_{abs,\lambda} C_{XT}$ to yield [34,39]

$$G_{\lambda,simp}(z) = q_{\lambda,0}\left[e^{-\bar{A}_{abs,\lambda}C_{XT}z} + \rho_\lambda e^{-\bar{A}_{abs,\lambda}C_{XT}(2L-z)}\right]. \quad (13)$$

Moreover, the mean volumetric rate of photon absorption $\langle \mathcal{A}_V \rangle$ can be determined by averaging the local volumetric rate of photon absorption $\mathcal{A}_V(z)$ over the volume of the PBR [22]. For a flat plate PBR of thickness L it is expressed as

$$\langle \mathcal{A}_V \rangle = \frac{1}{L}\int_0^L \mathcal{A}_V(z)dz = \frac{1}{L}\int_{400}^{700}\int_0^L C_{XT}\ \bar{A}_{abs,\lambda} G_\lambda(z)dzd\lambda. \quad (14)$$

Here, the local rate of photon absorption (LRPA) corresponds to the rate of photons absorbed at depth z in the PAR region between 400 and 700 nm, expressed per unit of time and dry biomass concentration. Finally, the growth kinetics of microalgae is related to the mean specific rate of photon absorption denoted by $\langle \mathcal{A} \rangle$ and expressed in $mol_{h\nu}$/kgh [16,21,22] and given by $\langle \mathcal{A} \rangle = \langle \mathcal{A}_V \rangle / C_{XT}$.

It is important to note that the simplified local fluence rate $G_{\lambda,simp}(z)$ given by Eq. (13) can be used in Eq. (14) to calculate analytically the corresponding simplified averaged volumetric rate of photon absorption $\langle \mathcal{A}_V \rangle_{simp}$ and the simplified LRPA $\langle \mathcal{A} \rangle_{simp}$ such that

$$\langle \mathcal{A}_V \rangle_{simp} = \frac{1}{L}\int_{400}^{700}\int_0^L C_{XT}\ \bar{A}_{abs,\lambda} G_{\lambda,simp}(z)dzd\lambda \text{ and } \langle \mathcal{A} \rangle_{simp} = \frac{\langle \mathcal{A}_V \rangle_{simp}}{C_{XT}}. \quad (15)$$

3. Materials and methods

3.1. Species and culture

Wild type *Chlamydomonas reinhardtii* strain 137 AH was obtained from the culture collection of the French Atomic Energy Agency (CEA, Cadarache, France). A culture of this *C. reinhardtii* strain was grown in a 1.5 L torus-shaped photobioreactor (PBR) made of transparent polymethyl methacrylate (PMMA) and operated in batch mode under progressive nitrogen starvation and autotrophic conditions using a modified artificial medium based on Sueoka medium. The used medium had the following composition (in g/L): NH_4Cl 0.1, $MgSO_4{\cdot}7H_2O$ 0.14, $CaCl_2{\cdot}H_2O$ 0.05, KH_2PO_4 0.3050, $NaHCO_3$ 1.68 and 1 mL/L of Hunter's trace elements solution. The illumination was provided by a LED panel and a light calibration curve to achieve a collimated incident photon flux $q_{\lambda,0}$ of 200 $\mu mol_{h\nu}/m^2$ s on the PBR. The latter was stirred constantly at 300 rpm. It was instrumented to monitor the pH, temperature, and dissolved O_2 in the liquid phase. Proportional-integral (PI) control was implemented for the regulation of these parameters. The pH was maintained at 7.5 *via* automatic CO_2 gas injection while the dissolved O_2 in the liquid phase was kept at 130% of oxygen saturation in air by injecting a gas mixture composed of 4.5 mol.% O_2 and 95.5 mol.% N_2. The inoculum used for launching the batch culture was obtained from a nitrogen-replete continuous culture in 1 L-airlift PBR operated under autotrophic conditions. Here also, the pH was regulated at 7.5 and the incident photon flux $q_{\lambda,0}$ was 200 $\mu mol_{h\nu}/m^2 s$.

3.2. Progressive nitrogen starvation strategy

The amount of inorganic nitrogen source (NH_4Cl) provided in the culture medium supports the biosynthesis of about 0.25–0.3 g/L of biomass before starch accumulation according to the stoichiometric equation for *C. reinhardtii* growth [16]. Thus, the culture dynamic of *C. reinhardtii* shows first a growth phase in which microalgae consume the sole inorganic nitrogen source available to sustain cell division followed by a carbon reserve accumulation phase once the nitrogen source is finally depleted. The initial concentration of NH_4Cl = 0.1 g/L was chosen to ensure that nitrogen starvation was the only parameter affecting carbon reserve storage and that no limitation due to light transfer may occur during the culture.

3.3. Physiological dynamics characterization

In order to study the dynamics of starch accumulation during progressive nitrogen starvation, the following biophysical parameters of the culture were measured at regular time intervals during the batch process: (i) the total and catalytic biomass expressed as dry weight (in kg/m^3), (ii) the cell density N_T (in #/mL), (iii) the Chl *a* and *b* and total carotenoid concentrations (in kg/m^3) and mass fractions, (iv) the starch concentration (kg/m^3) and mass fraction, (v) the concentration of inorganic nitrogen (ammonium NH_4^+) in the culture (in mg/L).

3.3.1. Total and catalytic biomass concentrations

The microalgae total dry weight biomass C_{XT} was measured by a gravimetric technique. A volume of culture, ranging from 5 to 15 mL, depending on the cell concentration, was filtered using a pre-dried and pre-weighed 0.7 µm pore size glass-microfiber filter (Whatman GF/F). The filters were dried at 110 °C for 24 h, cooled in a desiccator for 25–30 min and reweighed. The reported biomass concentration for each sample corresponded to the average of triplicates and the error bars correspond to 95% confidence intervals.

The total biomass C_{XT} is typically used as representative of the number of cells when microalgae are cultivated under non-limiting growth conditions. However, when *C. reinhardtii* is cultivated under nitrogen starvation conditions, cell division stops while carbon reserves are accumulated with concentration C_r. This means that the catalytic biomass concentration C_{XC} corresponding to the active fraction of the total biomass should be assumed as the referent of the number of cells in such a case since the accumulation of carbon reserves in the form of starch or lipids can modify the overall weight of an individual cell, although it does not necessarily imply that the cell density increases (Fig. 1A). Thus, the catalytic biomass C_{XC} which should remain proportional to the cell number density is defined as [22]

$$C_{XC} = C_{XT} - C_r = C_{XT} - (C_{st} + C_{TAG}). \quad (16)$$

This representation is particularly important because the radiation characteristics as well as the rates of light absorption can be now expressed per kg of C_{XC}.

Moreover, note that the starch and TAG accumulation phases are separated in time, as demonstrated in Refs. [8–10]. Thus, during the starch-accumulation phase, the carbon reserve concentration C_r corresponds only to the starch concentration, *i.e.*, $C_r = C_{st}$ and $C_{XC} = C_{XT} - C_{st}$. In addition, batch culture was carried out in the starch-accumulation phase throughout the progressive nitrogen starvation conditions. Moreover, the TAG concentration C_{TAG} was measured at the end of the batch culture and did not change throughout the cultivation. In other words, the TAG-accumulation phase was not observed.

3.3.2. Cell density, size distribution, and starch volume fraction

The cell density N_T (in #/mL) was measured by sampling the culture using a Malassez counting chamber and image software analysis ImageJ. The pictures were taken using a Zeiss microscope connected to a CCD camera (AxioScope A.1 with color camera AxioCam MRC, Zeiss) with total optical magnification of 400X (objective lens 40X and eyepiece 10X).

The size distribution of the cells was estimated at different stages of the batch culture by measuring the minor F_{min} and major F_{maj} Ferret diameters of individual cells treated as ellipsoids. *C. reinhardtii* cells were approximated as second order Tchebytchev

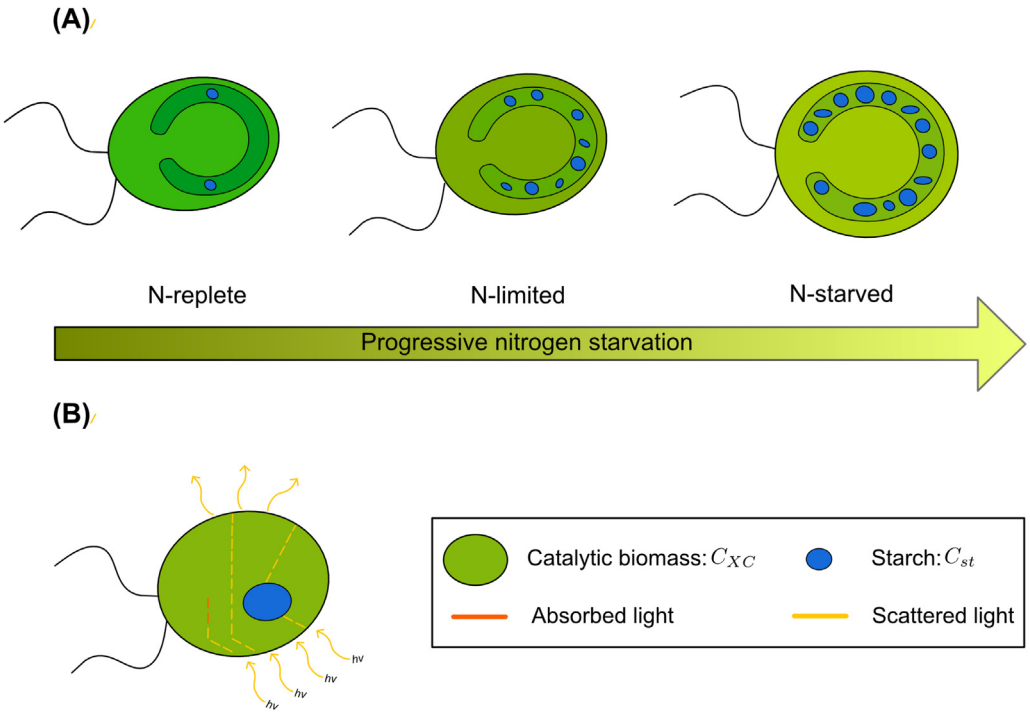

Fig. 1. Green microalgae cell *C. reinhardtii* compartmentalization into the catalytic biomass and the carbon reserves accumulated such as starch. (A) During progressive nitrogen starvation, the starch in the form of non-absorbing granules, is accumulated in the microalgae chloroplast, (B) The total biomass is composed of the catalytic biomass and accumulated starch. The first is responsible for the light absorption (red lines) and light scattering (yellow line), whereas the second is involved only in light scattering (yellow lines). The artificial or natural light is only absorbed by the catalytic biomass while the photons are scattered by the whole biomass, *i.e.*, the catalytic biomass and the starch.

particles (spheroids, $n = 2$) [16,40]. The Tchebytchev polynomial can describe a wider range of cell shapes. The volume-equivalent radius r_{eq} was defined as

$$r_{eq} = a_0 \sqrt[3]{T_v} \tag{17}$$

where, a_0 is the average diameter and T_v the Tchebytchev's polynomial, with both depending on the measured Ferret's diameters F_{min} and F_{maj} [41]. The frequency distribution of the volume-equivalent radius $f(r_{eq})$ was calculated according to

$$f(r_{eq}) = \frac{N(r_{eq})}{\int_0^\infty N(r_{eq})dr_{eq}} = \frac{N(r_{eq})}{N_T} \tag{18}$$

where, $N(r_{eq})$ is the number of cells per mL of suspension with a volume-equivalent radius between r_{eq} and $r_{eq} + \Delta r_{eq}$ with $\Delta r_{eq} = 0.1\ \mu$m. A minimum of 500 cells were analyzed for each size distribution presented and the reported error bars corresponded to 95% confidence intervals.

Finally, the experimental volume fraction of starch $f_{v,st}$ was estimated as

$$f_{v,st} = \frac{C_{st}}{N_T \rho_{st}} \tag{19}$$

where, ρ_{st} is the starch density taken as $\rho_{st} = 1.5$ kg/m^3 [42]. The reported experimental error bars of $f_{v,st}$ were calculated from propagating uncertainties in measuring microalgae starch concentration and the cell number, resulting in an estimated range of around 10–15%.

3.3.3. Pigment concentration and mass fraction

C. reinhardtii pigments were extracted in pure methanol and quantified using a spectrophotometer. A volume V_s of culture was centrifuged at 13,400 rpm for 15 min. The formed pellet with microalgae cells and pigments was resuspended in $V_{MeOH} = 1.5$ mL of pure methanol. The samples were incubated for 45 min to 1 h in an oven at 45 °C for extraction and then centrifuged for 10 min. Finally, the optical density (OD) of the supernatant was measured at wavelengths of 750, 665, 652, and 480 nm – corresponding to the absorption peaks of Chl *a* and *b* and carotenoids – using a UV-Vis spectrophotometer (Jasco V-730 Easton, MD). The pigment extractions were realized in triplicates and the reported value corresponds to the average. The reported error bars correspond to 95% confidence intervals. The concentrations C_{Chla} and C_{Chlb} in mg/L of photosynthetic pigments Chl *a* and *b* were determined using the widely used correlations [43]

$$C_{Chla} = [-8.0962(OD_{652} - OD_{750}) + 16.5169(OD_{665} - OD_{750})]V_{MeOH}/V_s. \tag{20}$$

$$C_{Chlb} = [27.4405(OD_{652} - OD_{750}) - 12.1688(OD_{665} - OD_{750})]V_{MeOH}/V_s. \tag{21}$$

The concentration C_{PPC} of total carotenoids (PPC) accounting for both photoprotective (PhPC) and photosynthetic (PSC) carotenoids was calculated according to [44]

$$C_{PPC} = 4(OD_{480} - OD_{750})V_{MeOH}/V_s. \tag{22}$$

The ratio of PhPC and PSC concentrations was considered to be constant and equal to 6 for all growth conditions [45].

Finally, the mass fractions of the different pigments were defined with respect to the total C_{XT} and catalytic C_{XC} biomass concentrations, respectively denoted by w_{pig} and w'_{pig} and expressed as

$$w_{pig} = \frac{C_{pig}}{C_{XT}} \text{ and } w'_{pig} = \frac{C_{pig}}{C_{XC}}. \tag{23}$$

3.3.4. Starch concentration and mass fraction

The white pellet remaining at the end of the pigment extraction and containing microalgae cells and starch was resuspended in a

sodium acetate buffer solution (0.1 M, pH = 4.5) and autoclaved at 135 °C for 1 h. Then, the samples were agitated and the starch concentration was measured with the commercial starch enzymatic assay kit SA-20 (Sigma-Aldrich). Measurements of the microalgal starch concentration C_{st} were performed in triplicates and the reported error bars correspond to 95% confidence intervals. Then, the starch mass fraction w_{st} was determined according to

$$w_{st} = \frac{C_{st}}{C_{XT}}. \tag{24}$$

3.3.5. Inorganic nitrogen (NH_4^+) concentration in the culture

The commercial spectrophotocolorimetric kits HACH Lange LCK 303 and LCK 305 were used for measuring the NH_4^+ ion concentration in the culture medium. A volume of culture between 0.2 mL to 5 mL was filtered in a 0.2 µm pore size single use filter unit (Minisart, Sartorius) and added to the kit's vials and incubated for 15 min at ambient temperature. Then, concentration was determined by a dedicated spectrophotometer (HACH Lange DR2800) measuring the absorbance at 695 nm.

3.4. Radiation characteristics

3.4.1. Experimental measurements

The experimental radiation characteristics $\bar{A}_{abs,\,\lambda}$ and $\bar{S}_{sca,\lambda}$ of *C. reinhardtii* under a progressive nitrogen starvation conditions and accumulating starch were measured at regular time intervals using the methodology described previously in Ref. [18]. First, the microalgae cells were washed and resuspended in PBS solution after being centrifugated at 13,400 rpm for 10–15 min. The normal-normal and normal-hemispherical transmittances $T_{nn,\lambda}$ and $T_{nh,\lambda}$ of the PBS-suspended cells were measured with a UV-Vis-NIR spectrophotometer (Agilent, Cary 5000, Santa Clara, CA) equipped with an integrated sphere module attachment (Agilent Cary DRA-2500, Santa Clara, CA). Here, the culture samples were diluted such that $C_{XT} \leq 0.13$ g/L to ensure that single scattering prevailed [18]. The measurements were performed in 1 cm path length quartz cuvettes (110-10-40 Hellma Analytics, Müllheim, Germany) at wavelengths between 400 and 750 nm. The spectral mass cross-sections of *C. reinhardtii* were measured for three different dry biomass concentrations C_{XT} to verify that they were independent of C_{XT}. It is important to note that the measured mass absorption cross-section was determined by replacing the total biomass C_{XT} with the catalytic biomass C_{XC} concentration in Eq. (1) such as $\bar{A}_{abs,\,\lambda} = \kappa_\lambda / C_{XC}$ since only the catalytic portion composed of the pigments and the constituents carbohydrates and lipids are involved in the absorption of the radiant energy necessary for growth and metabolite production (Fig. 1B) [22]. Contrary to absorption, scattering is caused by the entire cell composed of both the catalytic biomass and the carbon reserves (Fig. 1B). Then, the scattering cross-section $\bar{S}_{sca,\lambda}$ was defined based on the total biomass concentration C_{XT}, *i.e.*, $\bar{S}_{sca,\,\lambda} = \sigma_{s,\lambda} / C_{XT}$. Finally, depending on the inorganic nitrogen concentration measured, the experimental radiation characteristics were calculated using the correction factor (i) $\varepsilon_n = 0.67$ during normal growth conditions, *i.e.*, when ammonium was still available and (ii) $\varepsilon_n = 0.72$ during nitrogen deficiency conditions, based on a previous study [35]. The reported results of absorption and scattering mass cross-sections corresponded to the average of the triplicate measurements and the error bars to 95% confidence intervals.

3.4.2. Theoretical predictions

The theoretical radiation characteristics of *C. reinhardtii* under progressive nitrogen starvation and starch accumulation conditions were predicted based on the method developed in Ref. [26] and previously described. The total biomass C_{XT}, pigment $C_{pig,j}$, and starch C_{st} concentrations measured experimentally were used to predict the cells effective complex index of refraction $m_\lambda = n_\lambda + ik_\lambda$, as illustrated in Fig. 2. The cells effective absorption index k_λ was calculated according to

$$k_\lambda = \frac{\lambda}{4\pi} \sum_j C_{pig,\,j} E a_j = \frac{\lambda}{4\pi} \rho_{dry} (1 - x_w) \sum_j w'_{pig,\,j} E a_j \tag{25}$$

where, individual pigments Chl *a*, Chl *b*, and total catenoids PPC accounting for both photoprotective and photosynthetic carotenoids were considered.

The anchor refractive index n_{v_p} of *C. reinhardtii cells* accumulating carbon reserves was expressed as a weighted sum of the refractive indices of the cell constituents such that [36]

$$n_{v_p} = \sum n_j f_{v,\,j} = n_{basal}(1 - f_{v,st}) + n_{st}\ f_{v,st} + n_{TAG}\ f_{v,TAG} \tag{26}$$

where, f_{vj} is the volume fraction of the jth cellular compartment given by $f_{vj} = V_j / V_{cell}$ with V_{cell} being the total cell volume, *i.e.*, $V_{cell} = \frac{4}{3}\pi r_{eq}^3$. Here, we consider a basal refractive index n_{basal} corresponding to that of nutritional unstressed microalgae cell so that $n_{basal} = 1.375$ and the refractive index of starch as $n_{st} = 1.51$ and that of TAG as $n_{TAG} = 1.49$ at 820 nm [36]. When *C. reinhardtii* cells are accumulating only starch as carbon reserves, n_{v_p} can be written as

$$n_{v_p} = (1 - f_{v,st}) n_{basal} + n_{st}\ f_{v,st}. \tag{27}$$

This value of n_{v_p} was used to predict the spectral refractive index n_λ of *C. reinhardtii* cells using the Kramers–Kronig relation [Eq. (10)]. Moreover, the volume fraction of starch $f_{v,st}$ was calculated based on the basal volume of microalgae cells $V_{basal} = 4\pi r_{basal}^3/3$ so that

$$f_{v,st} = \frac{V_{st}}{V_{cell}} = \frac{V_{st}}{V_{basal} + V_{st}}. \tag{28}$$

Here, V_{st} is the volume occupied by starch in the microalgae cells given by

$$V_{st} = \left(\frac{w_{st}}{1 - w_{st}}\right) \frac{m_{XC}}{\rho_{st}} \tag{29}$$

where m_{XC} corresponds to the mass of one individual cell assumed to be constant and equal to 73 pg/cell, as estimated from biomass concentration and cell count under non-limiting growth conditions. The basal mean equivalent radius r_{basal} was taken as 4.0 μm for *C. reinhardtii* [25,35,46].

Finally, the prediction of the log-normal size distribution $f(r_{eq})$ of the microalgae cells under different nitrogen starvation conditions were computed considering a constant standard deviation ($\sigma = 0.56$ µm) inferred from experimental observations and a mean equivalent radius $\bar{r}_{eq}$ expressed as a function of the starch mass fraction accumulated such that

$$\bar{r}_{eq} = \sqrt[3]{\frac{3V_{cell}}{4\pi}} = \sqrt[3]{\frac{3(V_{basal} + V_{st})}{4\pi}}. \tag{30}$$

The error bars associated with the numerical predictions of absorption and scattering cross-sections resulted from the propagation of uncertainties in measuring the microalgae biological compounds such as the catalytic biomass and the pigment concentrations. The reported error bars were estimated to be around ± 15–20%.

3.5. Light transfer in PBR

The catalytic biomass concentration C_{XC} was considered as representative of the cell number in the culture, as previously explained. Thus, the local fluence rates $G'_\lambda(z)$ and $G'_{\lambda,simp}(z)$ were determined by replacing the total biomass concentration C_{XT} with the catalytic biomass concentration C_{XC} in Eqs. (11) and (13), respectively. In addition, the reflectance ρ_λ of the PMMA torus flat-panel

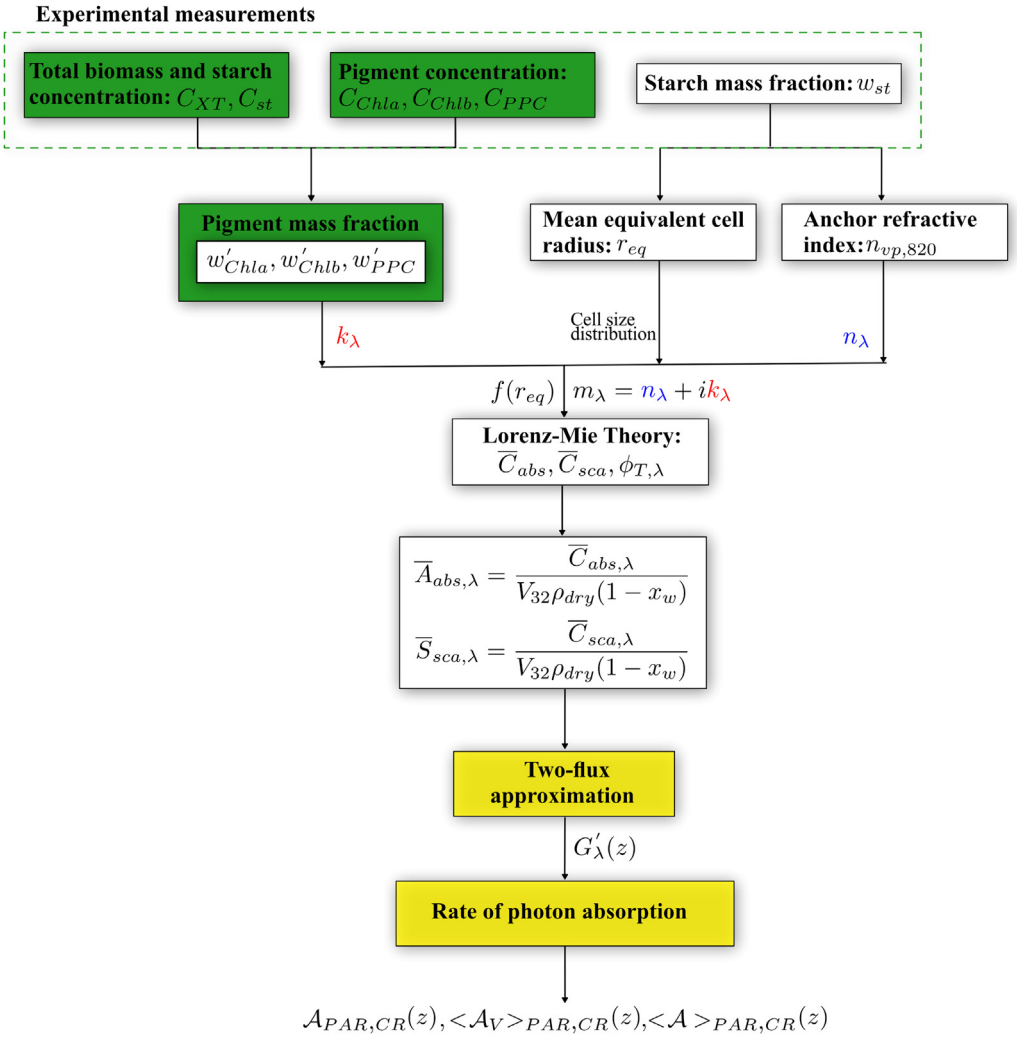

Fig. 2. Theoretical method developed for predicting microalgae radiation characteristics ($\bar{A}_{abs,\lambda}$ and $\bar{S}_{sca,\lambda}$) and the light absorption rate of microalgae culture in PBR under progressive nitrogen starvation conditions and accumulating carbon reserves. The method uses the total biomass, starch and pigment concentrations to establish the effective complex refractive index m_λ and the microalgae size distribution $f(r_{eq})$. The cross-sections ($\bar{C}_{abs,\lambda}$ and $\bar{C}_{sca,\lambda}$) and phase function $\Phi_{T,\lambda}(\Theta)$ are calculated using the Lorenz–Mie Theory. From these, radiations characteristics are determined and the backward scattering ratio b_λ can be estimated from the phase function (but assumed constant in this work). Then, the predicted radiation characteristics are used to calculate the fluence rate $G'_\lambda(z)$ and the rates of photon absorption.

PBR with a stainless steel back wall was taken as 0.2 [33]. The backward scattering ratio b_λ was assumed constant over the PAR region and equal to 0.008 [35].

The local spectral rate of photon absorption (LRPA) $\mathcal{A}_\lambda(z)$ which represents the amount of photons absorbed per unit of catalytic biomass and time at location z in the PBR. It depends on the *C. reinhardtii* average mass absorption cross-sections $\bar{A}_{abs,\lambda}$ and the local fluence rate $G'_\lambda(z)$ obtained under progressive nitrogen starvation conditions and accumulation of carbon reserves. It was calculated according to [17]

$$\mathcal{A}_\lambda(z) = \bar{A}_{abs,\lambda} G'_\lambda(z) \tag{31}$$

Moreover, the local PAR-averaged LRPA at location z can be expressed as

$$\mathcal{A}_{PAR,\ CR}(z) = \int_{400}^{700} \mathcal{A}_\lambda(z) d\lambda \tag{32}$$

Similarly, the PAR-averaged mean volumetric rate of photon absorption $\langle \mathcal{A}_V \rangle_{PAR}$ and the mean specific rate of photon absorption of microalgae culture in the PBR $\langle \mathcal{A} \rangle_{PAR}$ can be defined in terms of catalytic biomass concentration C_{XC} according to

$$\langle \mathcal{A}_V \rangle_{PAR,CR} = \frac{1}{L} \int_{400}^{700} \int_0^L C_{XC}\, \bar{A}_{abs,\lambda} G'_\lambda(z) dz d\lambda. \text{ and } \langle \mathcal{A} \rangle_{PAR,CR} = \frac{\langle \mathcal{A}_V \rangle_{PAR,CR}}{C_{XC}}. \tag{33}$$

Note that Eqs. (31)–(33) can be used to obtain the simplified rates of photon absorption $\mathcal{A}_{PAR,CR,simp}$, $\langle \mathcal{A}_V \rangle_{PAR,CR,simp}$ and $\langle \mathcal{A} \rangle_{PAR,CR,simp}$ by replacing the fluence rate given by the two-flux approximation $G'_\lambda(z)$ with a simplified two-flux approximation term $G'_\lambda(z)_{simp}$.

4. Results and discussion

4.1. Physiological dynamics

4.1.1. Biomass, NH_4^+ concentration and cell count

Fig. 3A and B show the temporal evolution of the total biomass C_{XT}, the catalytic biomass C_{XC}, the ammonium concentration $[NH_4^+]$ (in mg/L), and the total cell number density N_T during a progressive nitrogen starvation batch culture. They indicate that the total biomass concentration C_{XT} increased all along the exper-

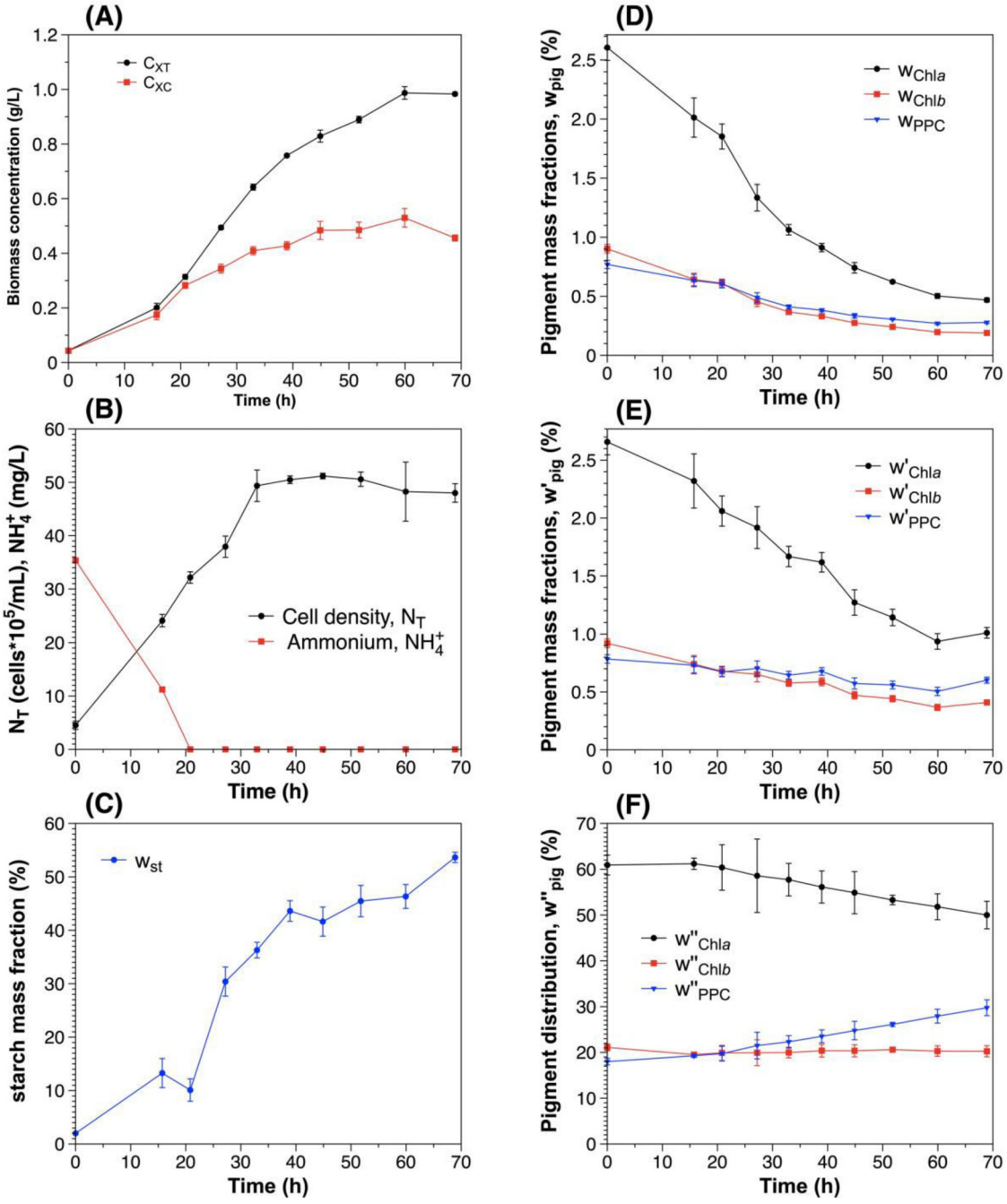

Fig. 3. Physiological changes of *C. reinhardtii* batch culture under a progressive nitrogen starvation condition. Temporal evolution of (A) the total C_{XT} and catalytic C_{XC} biomass concentrations, (B) ammonium concentration and cell density, and (C) starch mass content. Temporal evolution of (D) the pigment mass fractions in the total biomass w_{pig}, (E) the pigment mass fraction in the catalytic biomass w'_{pig}, and of (F) the pigment distribution w''_{pig}.

Table 1
Experimental measurements of four physiological states during a progressive nitrogen starvation batch culture.

Time (h)	NH_4^+ (mg/L)	w_{st}	$f_{v,st}$	$\bar{r}_{eq}$(μm)	w'_{Chla}	w'_{Chlb}	w'_{PPC}	w_{Chla}	w_{Chlb}	w_{PPC}
16	11.2	0.133	0.03	4.00 ± 0.49	2.7	0.9	0.8	2.7	0.9	0.8
27	0	0.304	0.11	3.88 ± 0.51	1.9	0.7	0.7	1.3	0.5	0.5
52	0	0.455	0.18	4.17 ± 0.60	1.1	0.4	0.6	0.6	0.2	0.3
69	0	0.536	0.22	4.31 ± 0.65	1.0	0.4	0.6	0.5	0.2	0.3

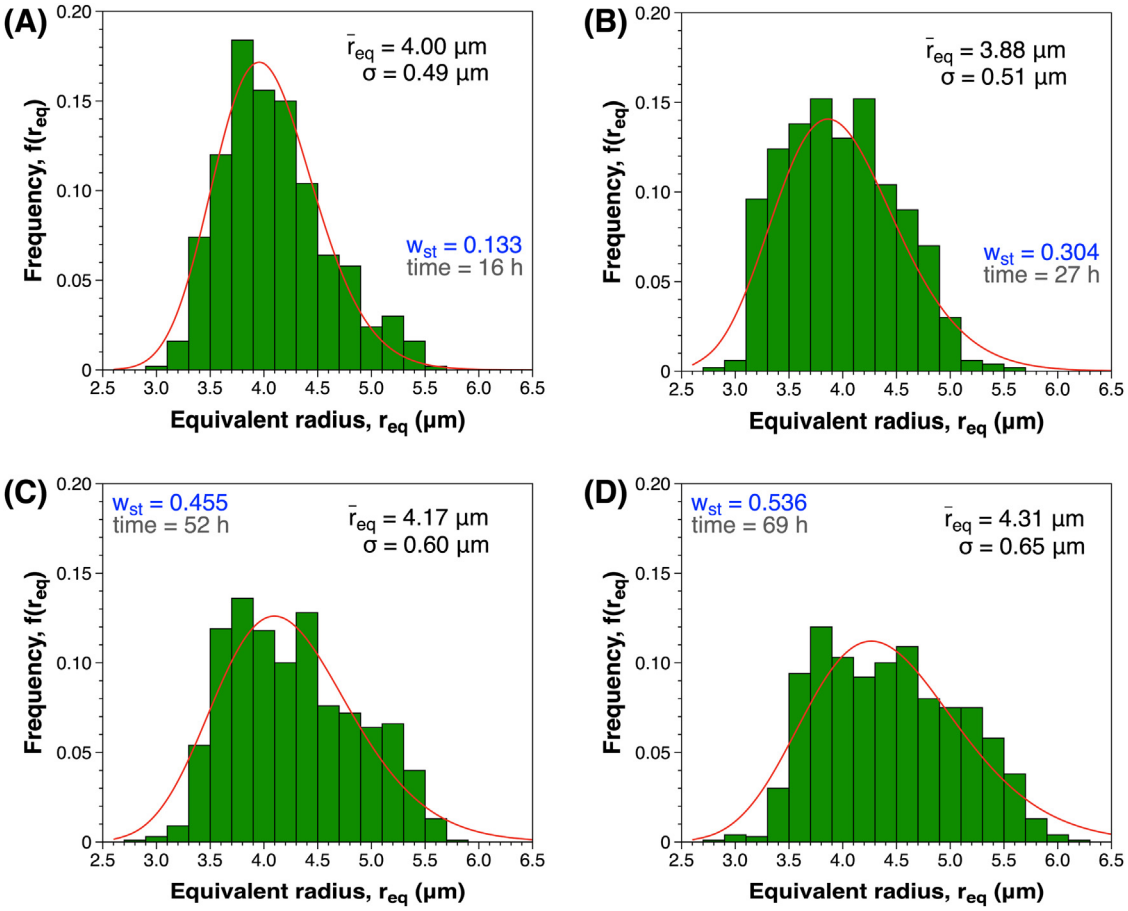

Fig. 4. Measured cell size distribution $f(r_{eq})$ and fitted log-normal distribution of *C. reinhardtii* under progressive nitrogen starvation in batch culture for different starch mass fractions namely (A) w_{st} = 0.133 after 16 h, (B) w_{st} = 0.304 after 27 h, (C) w_{st} = 0.455 after 52 h, and (D) w_{st} = 0.536 after 69 h.

iment up to 1 g/L after 69 h of culture. However, inorganic nitrogen concentration in the form of NH_4^+, necessary for cell division, was entirely consumed after 21 h. At that moment, the catalytic biomass concentration C_{XC} was approximately 0.3 g/L. This concentration is consistent with the fact that the ammonium initial load of 1.87 mM could theoretically sustain the biosynthesis of up to 0.25 g/L of biomass under standard growth conditions, according to the known stoichiometric relationship for non-limited growth of *C. reinhardtii* [16].

Moreover, microalgae cell number density N_T increased during the first 33 h, when cell division took place even after 21 h when nitrogen was totally consumed. Under nitrogen starvation conditions, some supplementary cell divisions may occur as microalgae cells are able to remobilize proteins of ribosomes and RuBisCO stocks [10,47]. After 33 h of culture, with nitrogen-deficient conditions, cell division stopped and the number of cells remained relatively unchanged. Thus, the total biomass concentration C_{XT} did not follow the same dynamic as the number of cells N_T due to starch accumulation inside the cells, as discussed in the next section. Therefore, the catalytic biomass concentration C_{XC} is the most relevant mass representation of the number of cells within the cultivation system. In fact, the catalytic biomass increased up to 0.4 g/L during the first 33 h of culture and remained between 0.4 and 0.5 g/L after cell division stopped.

4.1.2. Starch mass fraction

Fig. 3C shows the evolution of the starch mass fraction w_{st} during progressive nitrogen starvation in batch culture. The starch content reached up to 54% after 69 h. This result is consistent with the larger starch mass fraction w_{st} reported for *Chlamydomonas* microalgae species [48]. The starch content dynamic was related to the nitrogen deficiency and increased sharply after 21 h when inorganic nitrogen was consumed. Nevertheless, the starch accumulation phase seemed to have started even before 21 h when the microalgae culture was nitrogen-limited. Thus, the sustainable increase of total biomass concentration during the 69 h of batch culture despite the observed inorganic nitrogen consumption after 21 h can be explained by the carbon reserves accumulation process triggered inside the microalgae cells in the form of starch. *C. reinhardtii* cells can store starch and lipids during nitrogen-limiting conditions, as previously mentioned. However, they are accumulated separately in time with the starch storage phase occurring before the lipid production phase [8–10]. In fact, starch serves as a precursor for lipid synthesis if the nitrogen deprivation persists over time [11,49].

4.1.3. Pigment mass fractions

Fig. 3D to F describe the temporal evolution of the pigment mass fractions w_{pig} and w'_{pig} and of the pigment distribution $w''_{pig} = C_{pig}/C_{T,pig}$ such that $\sum w''_{pig} = 1$. Fig. 3D indicates that a significant decrease in the chlorophyll mass fractions w_{chla} and w_{chlb} in the total biomass. In fact, w_{chla} decreased by more than 5.5 times and w_{chlb} decreased by more than 4.7 times from their initial values measured at the beginning of the batch culture. Simultaneously, w_{PPC} decreased by more than 2.7 times. This decline in the pigment mass fractions w_{pig} can be explained by the progressive ni-

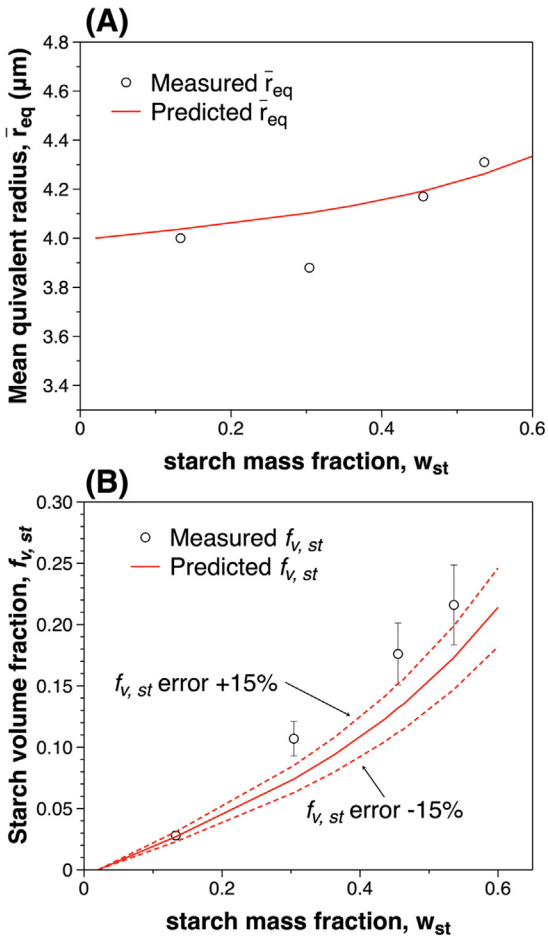

Fig. 5. Comparison of the theoretical predictions and experimental measurements of (A) the mean equivalent radius $\bar{r}_{eq}$ and (B) the starch volume fraction $f_{v,st}$ in microalgae cells for different starch mass fractions accumulated during progressive nitrogen starvation in a batch culture.

trogen starvation in which pigment adaptation take place in order to protect microalgae cells from light-induced oxidative stress by reducing the size of the photosynthetic antenna [20,21,50]. Nonetheless, this behavior can also be influenced by a dilution effect of pigments with respect to the total biomass concentration due to starch accumulation. In fact, chlorophyll mass fraction in nitrogen-starved cells fell because of the rapid cessation of their synthesis rather than because of their rapid degradation [5]. Thus, the evolution of the pigment mass fractions w'_{pig} in the catalytic biomass C_{XC} is more appropriate to analyze the dynamics of pigment contents in relation to the number of cells. Indeed, Fig. 3E reveals that the Chl *a* mass fraction w'_{chla} in the catalytic biomass declined by a factor 2.7 and Chl *b* mass fraction w'_{chlb} decreased by a factor 2 from the beginning of the batch culture. Simultaneously, the PPC mass fraction w'_{PPC} decreased from 0.78 to 0.6%, *i.e.*, by a factor 1.3. Note that the concentration ratio of Chl *a* to Chl *b* pigments was approximately constant around $C_{chla}/C_{chlb} = 2.8$ during the entire batch culture, despite the decrease in w'_{chl}, as observed in Ref. [8]. Therefore, *C. reinhardtii* cells adapted to progressive nitrogen starvation conditions by decreasing their chlorophyll mass fractions which stabilized by the end of the batch culture.

Fig. 3F shows the temporal evolution of the pigment distribution w''_{chla}, w''_{chlb}, and w''_{PPC}. All three distributions remained constant until the nitrogen was completely consumed. Once the nitrogen deficiency was reached after 21 h, the Chl *a* mass fraction w''_{chla} decreased progressively by 10% after 69 h of culture while the PPC mass fraction w''_{PPC} increased by the same percentage. The dynamic observed of the pigment distribution w''_{pig} did not stabilize over time, unlike the pigment mass fractions w_{pig} (Fig. 3A) and w'_{pig} (Fig. 3B). It is worth noting that the observed chlorophyll degradation in cells during nitrogen starvation (Fig. 3E) led to an increase in the PPC content w''_{PPC} within the pigment pool (Fig 3F) as carotenoids synthesis did not seem to be affected by the cultivated conditions, their concentration remained roughly constant throughout the duration of the culture (Fig. 3E). Thus, from a macroscopic perspective, the regulation of light absorption from microalgae cells during progressive nitrogen starvation appeared to be controlled by the decline in the chlorophyll mass fractions w'_{chla} and w'_{chlb} and by the acclimation of pigment distribution w''_{chla} and w''_{PPC}.

4.2. Comparison of theoretical and experimental radiation characteristics

For this comparison four different physiological states during the progressive nitrogen starvation batch culture were analyzed and are summarized in Table 1.

4.2.1. Measurements of cell size distribution and starch volume fraction

Fig. 4 plots the histograms of the volume-equivalent radius frequency distributions $f(r_{eq})$ and the fitting log-normal distributions of *C. reinhardtii* at four different times and starch mass fractions w_{st} (Table 1). At the beginning of the batch culture, while nitrogen was still present in the culture medium, the mean equivalent radius $\bar{r}_{eq}$ was around $\bar{r}_{eq} = 4.0$ µm and corresponded to that of *C. reinhardtii* cultivated under optimal conditions (Fig. 4A), as reported previously in Refs. [26,35,46] but without measuring the carbon reserves. Indeed, at this moment, the starch content w_{st} was only 13% and the starch volume fraction $f_{v,st}$ was 3% (Table 1). Thus, the beginning of starch accumulation phase within the cells did not seem to affect their size distribution during the growth period.

Fig. 4B–D show the changes in the cell size distribution $f(r_{eq})$ observed during nitrogen starvation conditions. It indicates that the cell radius r_{eq} increased progressively between 4.0 to 6.0 µm as the starch content w_{st} within cells increased. Similarly, the number of cells with equivalent radius r_{eq} between 3.0 and 4.0 µm decreased as the small microalgae cells were not regenerated since cellular division stopped after 33 h (Fig. 3B). Therefore, the cell size distribution profile tended to flatten by the end of the culture. To the best of our knowledge, no change in the cell size distribution has been reported for *C. reinhardtii* during nitrogen starvation batch culture. Nonetheless, the variation of the measured mean equivalent radius $\bar{r}_{eq}$ from Fig. 4B–D was only 10%.

Finally, changes in the shape of *C. reinhardtii* from ellipsoidal cells to larger spherical cells were previously observed in a sulfur deprived culture for hydrogen production [51]. These changes were attributed to starch accumulation but no quantitative analysis was reported. Here, Table 1 reports the evolution of the starch volume fraction $f_{v,st}$ during the nitrogen deficiency batch culture and indicates that $f_{v,st}$ increased by up to 22%.

4.2.2. Theoretical predictions of cell mean radius and starch volume fraction

Fig. 5A compares the experimentally measured and theoretically predicted (Eq. (30)) cell equivalent mean radius $\bar{r}_{eq}$ as a function of the starch volume fraction w_{st}. It indicates that the cell mean radius $\bar{r}_{eq}$ increased with increasing starch mass fraction.

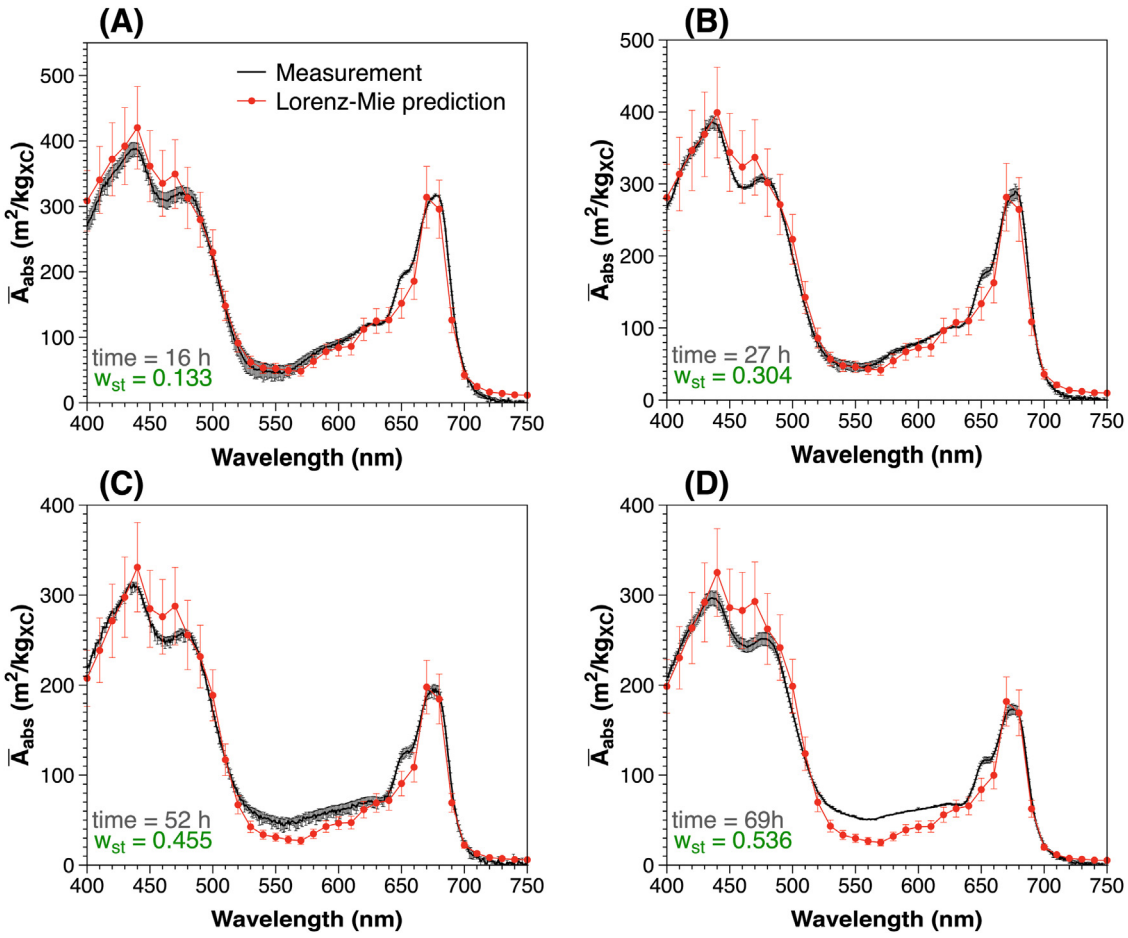

Fig. 6. Comparison between experimentally measured and theoretically predicted average spectral mass absorption cross-section $\bar{A}_{abs,\lambda}$ of *C. reinhardtii* under progressive nitrogen deprivation in batch culture for different starch mass fractions namely (A) w_{st} = 0.133 after 16 h, (B) w_{st} = 0.304 after 27 h, (C) w_{st} = 0.455 after 52 h, and (D) w_{st} = 0.536 after 69 h.

Overall, excellent agreement was observed between experimental results and theoretical predictions with an average relative error less than 3%. The larger discrepancy was observed for w_{st} = 0.304 and can be explained by the fact that, after 33 h of batch culture, the cell division took place under nitrogen deprivation. Then, the new cells were smaller than during normal division cycle.

Similarly, Fig. 5B compares the starch volume fraction $f_{v,st}$ vs. the starch mass fraction w_{st} obtained experimentally and predicted by Eq. (28). Reasonable agreements were observed between experiments and predictions. Note that $f_{v,st}$ was predicted considering a constant cell mass of 73 pg/cell. This value might need to be adjusted since, as the cell volume changes and starch accumulates during progressive nitrogen starvation, the mass of the cells should increase as well.

Finally, the anchor refractive index n_{v_p} predicted by Eq. (27) as a function of $f_{v,st}$ ranged between 1.375 and 1.40. The changes in the cell composition caused by starch accumulation did not significantly affect n_{v_p}. In fact, the reported values of n_{v_p} for a non-stressed *C. reinhardtii* culture were 1.375 [35,36,38] and 1.44 [26], and fell in the same range of that of *C. reinhardtii* cultivated during progressive nitrogen starvation in batch culture.

4.2.3. Measured vs. predicted mass absorption and scattering cross-sections

Fig. 6 compares the experimental measurements and the theoretical predictions of the spectral absorption cross-section $\bar{A}_{abs,\lambda}$ after (A) 16 h, (B) 27 h, (C) 52 h, and (D) 69 h of progressive nitrogen deprivation in a batch culture corresponding to different starch mass fractions w_{st}. It is evident that $\bar{A}_{abs,\lambda}$ decreased over time as nitrogen deprivation proceeded and pigment concentrations decreased (Fig. 3). The predicted average spectral mass absorption cross-section $\bar{A}_{abs,\lambda}$ agreed very well with the measurements across the PAR region and for all the physiological states investigated. In fact, the PAR-averaged relative difference between experimental measurements and theoretical predictions was less than 5%. Furthermore, the relative differences at wavelengths 440 nm and 676 nm, corresponding to the absorption peaks of chlorophylls *a* and *b*, did not exceed 10% for $\bar{A}_{abs,440}$ and 8% for the $\bar{A}_{abs,676}$.

Similarly, Fig. 7 compares the spectral scattering mass cross-section $\bar{S}_{sca,\lambda}$ measured and predicted at different times during progressive nitrogen starvation in a batch culture. It indicates that, unlike the absorption cross section $\bar{A}_{abs,\lambda}$, $\bar{S}_{sca,\lambda}$ remained nearly unchanged during the batch culture despite significant physiological changes (Fig. 3). Here also, the predictions and measurements agreed relatively well with a PAR-averaged relative difference of up to 18%. Overall, these results are good given the very complex physiological changes occurring to the cells under the studied cultivation conditions. Any discrepancies found between theoretical predictions and experimental measurements of the scattering mass cross-sections could be attributed to the fact that experimental measurements used the same correction factor ε_n during the accumulation phase of carbon reserves, once nitrogen source was totally consumed. However, a small difference in the correction factor ε_n was reported between *C. reinhardtii* cultures under

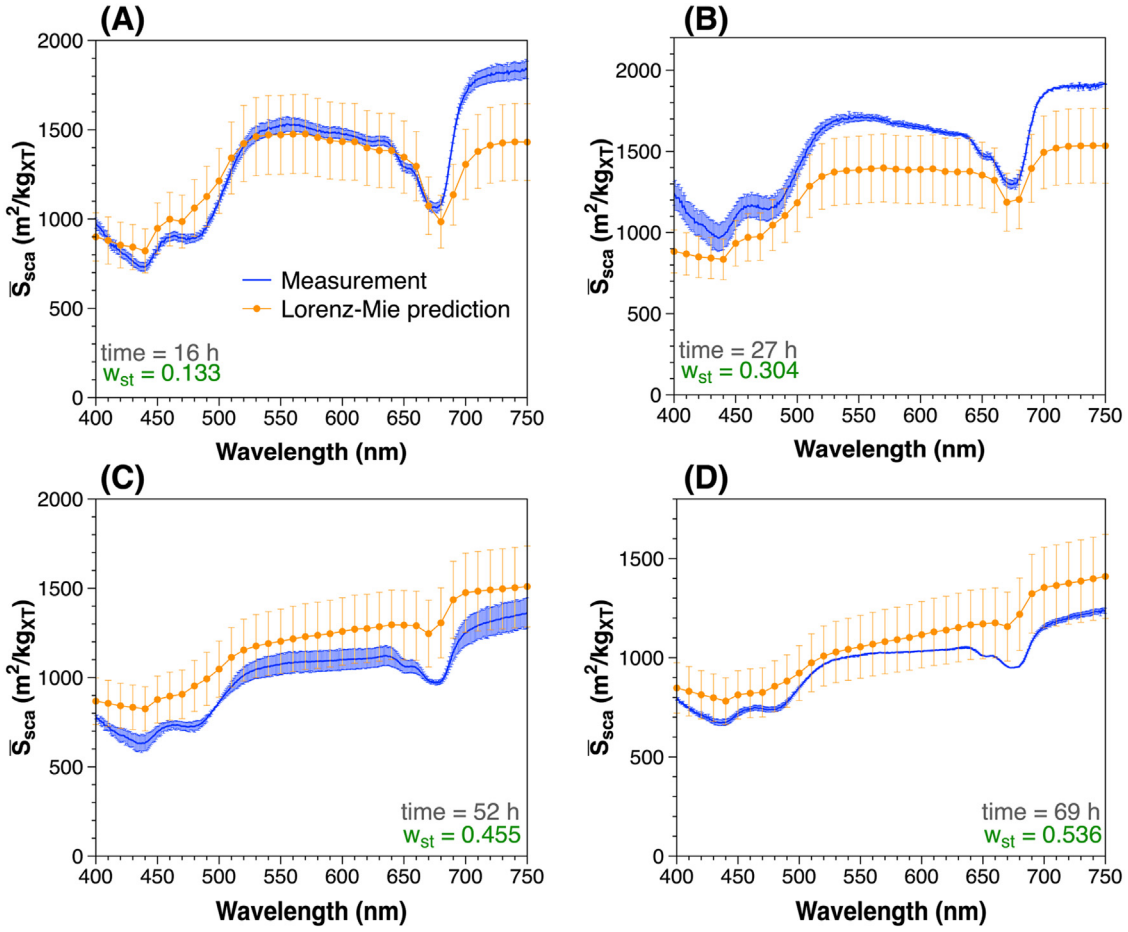

Fig. 7. Comparison between experimentally measured and theoretically predicted average spectral mass scattering cross-section $\bar{S}_{sca,\lambda}$ of *C. reinhardtii* under progressive nitrogen starvation in batch culture for different starch mass fractions namely (A) w_{st} = 0.133 after 16 h, (B) w_{st} = 0.304 after 27 h, (C) w_{st} = 0.455 after 52 h, and (D) w_{st} = 0.536 after 69 h.

non-limiting (ε_n = 0.67) and nitrogen-limiting (ε_n = 0.72) conditions [35].

4.2.4. Local rate of photon absorption (LRPA)

Fig. 8 compares the PAR-averaged local rate of photon absorption $\mathcal{A}_{PAR,CR}(z)$ and $\mathcal{A}_{PAR,CR,simp}(z)$ determined as functions of the PBR depth z using the complete or simplified two-flux approximation for the determination of $G'_{\lambda}(z)$ and $G'_{\lambda,simp}(z)$, and experimentally measured and theoretically predicted spectral radiation characteristics of the microalgae (See Figs. 6 and 7). Fig. 8 indicates that the PAR-averaged LRPA decreased during the batch culture as the pigment concentrations and the average mass absorption cross-section decreased.

To simplify citation, the terms 'experimentally determined PAR-averaged LRPA' and 'numerically determined PAR-averaged LRPA' were used to denote the PAR-averaged LRPAs calculated from experimentally measured or theoretically predicted radiations characteristics. Fig. 8 demonstrates a very good agreement between both the experimentally and numerically calculated PAR-averaged LRPA $\mathcal{A}_{PAR,CR}(z)$ as well as the simplified PAR-averaged LRPA $\mathcal{A}_{PAR,CR,simp}(z)$. Indeed, the PAR-averaged LRPA relative differences between experimental and numerical LRPAs were lower than 1% for the intermediate starch mass fraction ($w_{st} \leq 0.3$) and for the higher starch mass fraction, it ranged between 7 and 9% (Fig. 8).

In addition, Fig. 8 similarly shows that the PAR-averaged LRPA values obtained using a simplified two-flux approximation, $\mathcal{A}_{PAR,CR,simp}(z)$, were very similar to those obtained with a complete two-flux approximation, $\mathcal{A}_{PAR,CR}(z)$. In fact, the relative differences in the PAR-averaged LRPA between $\mathcal{A}_{PAR,CR}(z)$ and $\mathcal{A}_{PAR,CR,simp}(z)$ were found lower than 5% for the four different physiological states during the progressive nitrogen starvation culture. As previously explained, microalgae suspensions scatter visible light mostly in the forward direction so that the influence of $\bar{S}_{sca,\lambda}$ in the two-flux approximation and consequently, on the calculation of PAR-averaged LRPA is negligible [34,39]. The present results establish that this was also valid for nutritionally-deprived microalgae culture accumulating carbon reserves as starch. Therefore, the PAR-averaged LRPA values for a *C. reinhardtii* culture under nitrogen-limited conditions and accumulating carbon reserves could be estimated using the simplified two-flux approximation accounting only for the cell spectral absorption cross-section $\bar{A}_{abs,\lambda}$.

Overall, the methodology developed in this study is capable of predicting accurately the mass absorption $\bar{A}_{abs,\lambda}$ and scattering $\bar{S}_{sca,\lambda}$ cross-sections and the LRPA of a *C reinhardtii* culture in PBR cultivated under progressive nitrogen starvation conditions with intracellular accumulation of starch as carbon reserves.

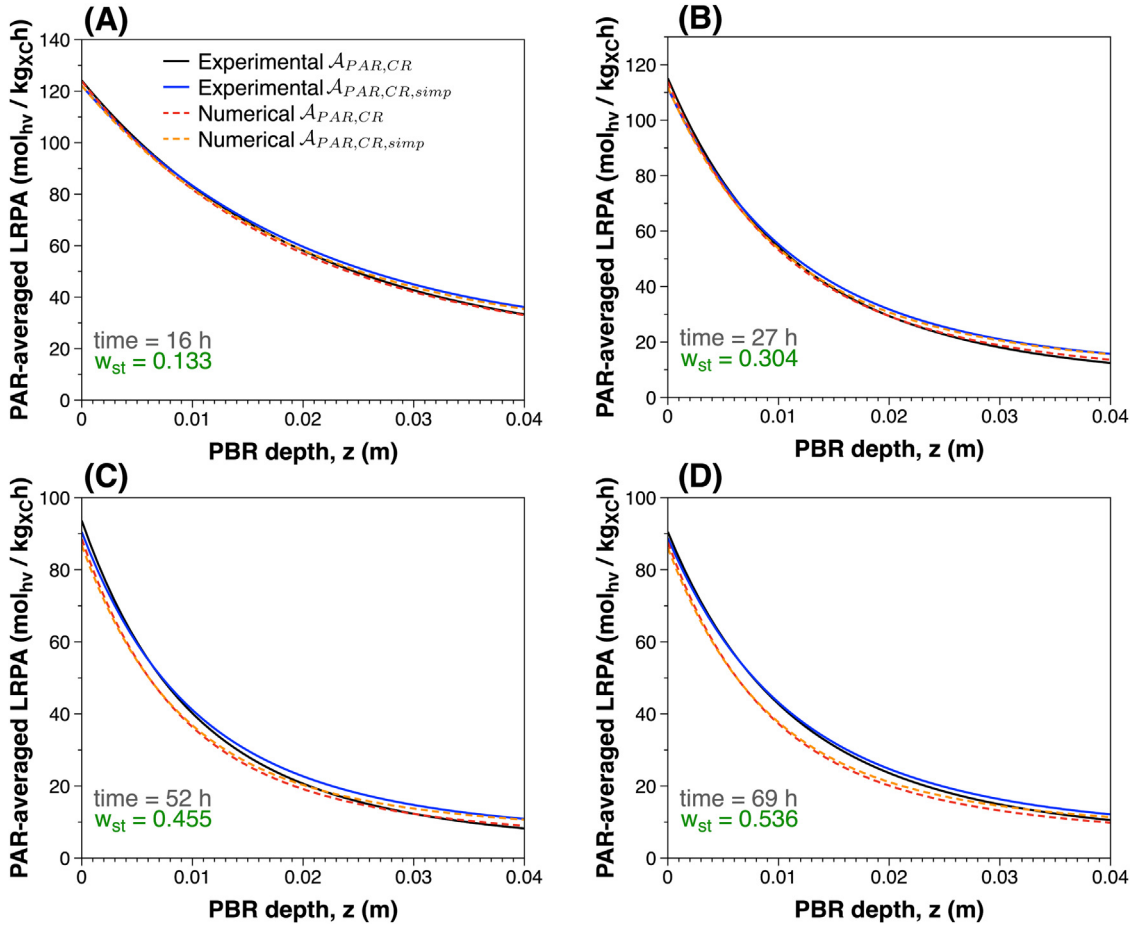

Fig. 8. Comparison of the PAR-averaged local rate of photon absorption LRPA $\mathcal{A}_{PAR,CR}(z)$ and simplified LRPA $\mathcal{A}_{PAR,CR,simp}(z)$ predicted using the complete or simplified two-flux approximation for the calculation of $G'_{\lambda}(z)$ and $G'_{\lambda,simp}(z)$, and experimentally measured and theoretically predicted radiation characteristics of *C. reinhardtii* under progressive nitrogen starvation in batch culture for different starch mass fractions namely (A) $w_{st} = 0.133$ after 16 h, (B) $w_{st} = 0.304$ after 27 h, (C) $w_{st} = 0.455$ after 52 h, and (D) $w_{st} = 0.536$ after 69 h.

5. Conclusion

This study developed and validated experimentally a method for predicting the radiation characteristics of the green microalgae *C. reinhardtii* cultivated under progressive nitrogen starvation in batch culture leading to accumulation of carbon reserves in the form of starch. Predictions of the spectral absorption index k_{λ} and the refractive index n_{λ} of N-starved microalgae cells took into account (*i*) the physiological changes including the decrease in pigment concentrations, the cessation of cell division, thanks to the introduction of the catalytic biomass concentration and (*ii*) the change in the volume of the microalgae cells caused by the accumulation of carbon reserves. Predictions of the N-deprived microalgae complex index of refraction $m_{\lambda} = n_{\lambda} + i\,k_{\lambda}$ and the measured cell size distribution were used in the Lorenz–Mie theory to obtain the spectral mass absorption and scattering cross-sections of cell. Moreover, the local rate of photon absorption could be predicted using the simplified two-flux approximation and the theoretically predicted absorption coefficient for all microalgae physiological states during a progressive nitrogen starvation. Finally, this methodology could be used to develop a database of radiation characteristics necessary for future microalgae kinetic modeling of carbon reserve accumulation under nitrogen-limiting conditions.

Funding

This work was supported by the French Ministry of Higher Education and Research.

Declaration of Competing Interest

The authors declare that they have no known competing financial interests or personal relationships that could have appeared to influence the work reported in this paper.

CRediT authorship contribution statement

Fernando Robert Ferrel Ballestas: Conceptualization, Methodology, Formal analysis, Investigation, Data curation, Writing – original draft, Visualization. **Mariana Titica:** Conceptualization, Methodology, Writing – review & editing, Supervision. **Jack Legrand:** Conceptualization, Methodology, Writing – review & editing, Supervision. **Laurent Pilon:** Conceptualization, Methodology, Formal analysis, Visualization, Writing – review & editing, Supervision. **Guillaume Cogne:** Conceptualization, Methodology, Writing – review & editing, Supervision.

References

[1] Borowitzka MA. High-value products from microalgae—Their development and commercialisation. J Appl Phycol 2013;25:743–56. doi:10.1007/s10811-013-9983-9.

[2] Udayan A, Pandey AK, Sharma P, Sreekumar N, Kumar S. Emerging industrial applications of microalgae: challenges and future perspectives. Syst Microbiol Biomanuf 2021;1:411–31. doi:10.1007/s43393-021-00038-8.

[3] Rumin J, Gonçalves de Oliveira Junior R, Bérard JB, Picot L. Improving microalgae research and marketing in the European Atlantic area: analysis of major gaps and barriers limiting sector development. Mar Drugs 2021;19:319. doi:10.3390/md19060319.

[4] Oncel SS. Microalgae for a macroenergy world. Renew Sustain Energy Rev 2013;26:241–64. doi:10.1016/j.rser.2013.05.059.

[5] Antal TK. The metabolic acclimation of *Chlamydomonas reinhardtii* to depletion of essential nutrients: application for hydrogen production. In: Seibert M, Torzillo G, editors. Microalgal hydrogen production: achievements and perspectives. Cambridge: Royal Society of Chemistry; 2018. p. 235–64. doi:10.1039/9781849737128-00235.

[6] Ran W, Wang H, Liu Y, Qi M, Xiang Q, Yao C, et al. Storage of starch and lipids in microalgae: biosynthesis and manipulation by nutrients. Bioresour Technol 2019;291:121894. doi:10.1016/j.biortech.2019.121894.

[7] de Carvalho Silvello MA, Severo Gonçalves I, Patrícia Held Azambuja S, Silva Costa S, Garcia Pereira Silva P, Oliveira Santos L, et al. Microalgae-based carbohydrates: a green innovative source of bioenergy. Bioresour Technol 2022;344:126304. doi:10.1016/j.biortech.2021.126304.

[8] Adesanya VO, Davey MP, Scott SA, Smith AG. Kinetic modelling of growth and storage molecule production in microalgae under mixotrophic and autotrophic conditions. Bioresour Technol 2014;157:293–304. doi:10.1016/j.biortech.2014.01.032.

[9] Longworth J, Noirel J, Pandhal J, Wright PC, Vaidyanathan S. HILIC- and SCX-based quantitative proteomics of Chlamydomonas reinhardtii during nitrogen starvation induced lipid and carbohydrate accumulation. J Proteome Res 2012;11:5959–71. doi:10.1021/pr300692t.

[10] Park JJ, Wang H, Gargouri M, Deshpande RR, Skepper JN, Holguin FO, et al. The response of Chlamydomonas reinhardtii to nitrogen deprivation: a systems biology analysis. Plant J Cell Mol Biol 2015;81:611–24. doi:10.1111/tpj.12747.

[11] Juergens MT, Deshpande RR, Lucker BF, Park JJ, Wang H, Gargouri M, et al. The regulation of photosynthetic structure and function during nitrogen deprivation in *Chlamydomonas reinhardtii*. Plant Physiol 2015;167:558–73. doi:10.1104/pp.114.250530.

[12] Chochois V, Dauvillée D, Beyly A, Tolleter D, Cuiné S, Timpano H, et al. Hydrogen Production in Chlamydomonas: photosystem II-Dependent and -Independent Pathways Differ in Their Requirement for Starch Metabolism. Plant Physiol 2009;151:631–40. doi:10.1104/pp.109.144576.

[13] Torzillo G, Scoma A, Faraloni C, Giannelli L. Advances in the biotechnology of hydrogen production with the microalga Chlamydomonas reinhardtii. Crit Rev Biotechnol 2015;35:485–96. doi:10.3109/07388551.2014.900734.

[14] Bekirogullari M, Figueroa-Torres GM, Pittman JK, Theodoropoulos C. Models of microalgal cultivation for added-value products - a review. Biotechnol Adv 2020;44:107609. doi:10.1016/j.biotechadv.2020.107609.

[15] Figueroa-Torres GM, Pittman JK, Theodoropoulos C. Kinetic modelling of starch and lipid formation during mixotrophic, nutrient-limited microalgal growth. Bioresour Technol 2017;241:868–78. doi:10.1016/j.biortech.2017.05.177.

[16] Takache H, Pruvost J, Cornet JF. Kinetic modeling of the photosynthetic growth of Chlamydomonas reinhardtii in a photobioreactor. Biotechnol Prog 2012;28:681–92. doi:10.1002/btpr.1545.

[17] Cornet JF, Dussap CG, Dubertret G. A structured model for simulation of cultures of the cyanobacterium Spirulina platensis in photobioreactors: I. Coupling between light transfer and growth kinetics. Biotechnol Bioeng 1992;40:817–25. doi:10.1002/bit.260400709.

[18] Pilon L, Berberoğlu H, Kandilian R. Radiation transfer in photobiological carbon dioxide fixation and fuel production by microalgae. J Quant Spectrosc Radiat Transf 2011;112:2639–60. doi:10.1016/j.jqsrt.2011.07.004.

[19] Pilon L, Kandilian R. Interaction between light and photosynthetic microorganisms. Adv. Chem. Eng. 2016;48:107–49 Elsevier. doi:10.1016/bs.ache.2015.12.002.

[20] Pruvost J, Van Vooren G, Cogne G, Legrand J. Investigation of biomass and lipids production with Neochloris oleoabundans in photobioreactor. Bioresour Technol 2009;100:5988–95. doi:10.1016/j.biortech.2009.06.004.

[21] Kandilian R, Pruvost J, Legrand J, Pilon L. Influence of light absorption rate by Nannochloropsis oculata on triglyceride production during nitrogen starvation. Bioresour Technol 2014;163:308–19. doi:10.1016/j.biortech.2014.04.045.

[22] Kandilian R, Taleb A, Heredia V, Cogne G, Pruvost J. Effect of light absorption rate and nitrate concentration on TAG accumulation and productivity of Parachlorella kessleri cultures grown in chemostat mode. Algal Res 2019;39:101442. doi:10.1016/j.algal.2019.101442.

[23] Van Vooren G, Le Grand F, Legrand J, Cuiné S, Peltier G, Pruvost J. Investigation of fatty acids accumulation in Nannochloropsis oculata for biodiesel application. Bioresour Technol 2012;124:421–32. doi:10.1016/j.biortech.2012.08.009.

[24] Hoeniges J, Kandilian R, Zhang C, Pruvost J, Legrand J, Grizeau D, et al. Effect of colony formation on light absorption by Botryococcus braunii. Algal Res 2020;50:101985. doi:10.1016/j.algal.2020.101985.

[25] Pottier L, Pruvost J, Deremetz J, Cornet JF, Legrand J, Dussap CG. A fully predictive model for one-dimensional light attenuation by Chlamydomonas reinhardtii in a torus photobioreactor. Biotechnol Bioeng 2005;91:569–82. doi:10.1002/bit.20475.

[26] Dauchet J, Blanco S, Cornet JF, Fournier R. Calculation of the radiative properties of photosynthetic microorganisms. J Quant Spectrosc Radiat Transf 2015;161:60–84. doi:10.1016/j.jqsrt.2015.03.025.

[27] Berberoglu H, Yin J, Pilon L. Light transfer in bubble sparged photobioreactors for H_2 production and CO_2 mitigation. Int J Hydrogen Energy 2007;32:2273–85. doi:10.1016/j.ijhydene.2007.02.018.

[28] Jonasz M, Fournier GR. Light scattering by particles in water: theoretical and experimental foundations. Light Scatt Part Water Theor Exp Found 2007. doi:10.1016/B978-0-12-388751-1.X5000-5.

[29] Kandilian R, Heng RL, Pilon L. Absorption and scattering by fractal aggregates and by their equivalent coated spheres. J Quant Spectrosc Radiat Transf 2015;151:310–26. doi:10.1016/j.jqsrt.2014.10.018.

[30] Heng RL, Sy KC, Pilon L. Absorption and scattering by bispheres, quadspheres, and circular rings of spheres and their equivalent coated spheres. JOSA A 2015;32:46–60. doi:10.1364/JOSAA.32.000046.

[31] Lee E, Pilon L. Absorption and scattering by long and randomly oriented linear chains of spheres. J Opt Soc Am A 2013;30:1892. doi:10.1364/JOSAA.30.001892.

[32] Harris EH, Stern DB, Witman GB. The chlamydomonas sourcebook. chlamydomonas sourceb. 2nd Ed. London: Academic Press; 2009. iii. doi:10.1016/B978-0-12-370873-1.00059-9.

[33] Takache H, Christophe G, Cornet JF, Pruvost J. Experimental and theoretical assessment of maximum productivities for the microalgae Chlamydomonas reinhardtii in two different geometries of photobioreactors. Biotechnol Prog 2010;26:431–40. doi:10.1002/btpr.356.

[34] Lee E, Pruvost J, He X, Munipalli R, Pilon L. Design tool and guidelines for outdoor photobioreactors. Chem Eng Sci 2014;106:18–29. doi:10.1016/j.ces.2013.11.014.

[35] Kandilian R, Pruvost J, Artu A, Lemasson C, Legrand J, Pilon L. Comparison of experimentally and theoretically determined radiation characteristics of photosynthetic microorganisms. J Quant Spectrosc Radiat Transf 2016;175:30–45. doi:10.1016/j.jqsrt.2016.01.031.

[36] Bhowmik A, Pilon L. Can spherical eukaryotic microalgae cells be treated as optically homogeneous? J Opt Soc Am A 2016;33:1495. doi:10.1364/JOSAA.33.001495.

[37] Bidigare RR, Ondrusek ME, Morrow JH, Kiefer DA. *In-vivo* absorption properties of algal pigments. Proc SPIE Ocean Opt X 1990;1302:290–302. doi:10.1117/12.21451.

[38] Lee E, Heng RL, Pilon L. Spectral optical properties of selected photosynthetic microalgae producing biofuels. J Quant Spectrosc Radiat Transf 2013;114:122–35. doi:10.1016/j.jqsrt.2012.08.012.

[39] Kandilian R, Soulies A, Pruvost J, Rousseau B, Legrand J, Pilon L. Simple method for measuring the spectral absorption cross-section of microalgae. Chem Eng Sci 2016;146:357–68. doi:10.1016/j.ces.2016.02.039.

[40] Mishchenko MI, Travis LD, Lacis AA. Scattering, absorption, and emission of light by small particles, 4. Cambridge University Press; 2002.

[41] Cornet JF. Procédés limités par le transfert de rayonnement en milieu hétérogène. habilitation à diriger des recherches. Université Blaise Pascal - Clermont-Ferrand II; 2007.

[42] Marousis SN, Saravacos GD. Density and porosity in drying starch materials. J Food Sci 1990;55:1367–72. doi:10.1111/j.1365-2621.1990.tb03939.x.

[43] Ritchie RJ. Consistent sets of spectrophotometric chlorophyll equations for acetone, methanol and ethanol solvents. Photosynth Res 2006;89:27–41. doi:10.1007/s11120-006-9065-9.

[44] Strickland JDH, Parsons TR. A practical handbook of seawater analysis. Fisheries Research Board of Canada; 1977.

[45] Dubinsky Z, Stambler N. Photoacclimation processes in phytoplankton: mechanisms, consequences, and applications. Aquat Microb Ecol 2009;56:163–76. doi:10.3354/ame01345.

[46] Berberoglu H, Pilon L, Melis A. Radiation characteristics of Chlamydomonas reinhardtii CC125 and its truncated chlorophyll antenna transformants tla1, tlaX and tla1-CW+. Int J Hydrogen Energy 2008;33:6467–83. doi:10.1016/j.ijhydene.2008.07.071.

[47] Zhang D, Vassiliadis VS. *Chlamydomonas reinhardtii* metabolic pathway analysis for biohydrogen production under non-steady-state operation. Ind Eng Chem Res 2015;54:10593–605. doi:10.1021/acs.iecr.5b02034.

[48] Gifuni I, Olivieri G, Pollio A, Franco TT, Marzocchella A. Autotrophic starch production by Chlamydomonas species. J Appl Phycol 2017;29:105–14. doi:10.1007/s10811-016-0932-2.

[49] Smythers AL, McConnell EW, Lewis HC, Mubarek SN, Hicks LM. Photosynthetic metabolism and nitrogen reshuffling are regulated by reversible cysteine thiol oxidation following nitrogen deprivation in chlamydomonas. Plants 2020;9:784. doi:10.3390/plants9060784.

[50] Kandilian R, Lee E, Pilon L. Radiation and optical properties of Nannochloropsis oculata grown under different irradiances and spectra. Bioresour Technol 2013;137:63–73. doi:10.1016/j.biortech.2013.03.058.

[51] Zhang L, Happe T, Melis A. Biochemical and morphological characterization of sulfur-deprived and H2-producing Chlamydomonas reinhardtii (green alga). Planta 2002;214:552–61. doi:10.1007/s004250100660.